

# Lamin A/C sustains PcG protein architecture, maintaining transcriptional repression at target genes

Elisa Cesarini,<sup>1</sup> Chiara Mozzetta,<sup>1</sup> Fabrizia Marullo,<sup>1</sup> Francesco Gregoretti,<sup>3</sup> Annagiusti Gargiulo,<sup>1</sup> Marta Columbaro,<sup>4</sup> Alice Cortesi,<sup>5</sup> Laura Antonelli,<sup>3</sup> Simona Di Pelino,<sup>5</sup> Stefano Squarzone,<sup>4,6</sup> Daniela Palacios,<sup>2</sup> Alessio Zippo,<sup>5</sup> Beatrice Bodega,<sup>5</sup> Gennaro Oliva,<sup>3</sup> and Chiara Lanzuolo<sup>1</sup>

<sup>1</sup>Consiglio Nazionale delle Ricerche Institute of Cellular Biology and Neurobiology, Istituto di Ricovero e Cura a Carattere Scientifico Fondazione Santa Lucia, 00143 Rome, Italy

<sup>2</sup>Istituto di Ricovero e Cura a Carattere Scientifico Fondazione Santa Lucia, 00143 Rome, Italy

<sup>3</sup>Consiglio Nazionale delle Ricerche Institute for High Performance Computing and Networking, 80131 Naples, Italy

<sup>4</sup>Struttura Complessa Laboratorio Biologia Cellulare Muscoloscheletrica, Istituto Ortopedico Rizzoli, 40136 Bologna, Italy

<sup>5</sup>Istituto Nazionale Genetica Molecolare Romeo ed Enrica Invernizzi, 20122 Milan, Italy

<sup>6</sup>Consiglio Nazionale delle Ricerche Institute of Molecular Genetics, 40136 Bologna, Italy

Beyond its role in providing structure to the nuclear envelope, lamin A/C is involved in transcriptional regulation. However, its cross talk with epigenetic factors—and how this cross talk influences physiological processes—is still unexplored. Key epigenetic regulators of development and differentiation are the Polycomb group (PcG) of proteins, organized in the nucleus as microscopically visible foci. Here, we show that lamin A/C is evolutionarily required for correct PcG protein nuclear compartmentalization. Confocal microscopy supported by new algorithms for image analysis reveals that lamin A/C knock-down leads to PcG protein foci disassembly and PcG protein dispersion. This causes detachment from chromatin and defects in PcG protein-mediated higher-order structures, thereby leading to impaired PcG protein repressive functions. Using myogenic differentiation as a model, we found that reduced levels of lamin A/C at the onset of differentiation led to an anticipation of the myogenic program because of an alteration of PcG protein-mediated transcriptional repression. Collectively, our results indicate that lamin A/C can modulate transcription through the regulation of PcG protein epigenetic factors.

## Introduction

The inner part of the nuclear envelope comprises a complex meshwork of proteins, known as lamins, which form the nuclear lamina (NL; Gruenbaum and Foisner, 2015). In vertebrates, lamin proteins have been divided into A and B types, based on sequence homologies. Whereas B-type lamins are ubiquitously expressed, A-type lamins, such as lamin A and C (hereafter lamin A/C), are developmentally regulated, being absent in the early embryo and expressed in differentiating cells (Stewart and Burke, 1987; Röber et al., 1989), suggesting a role in cell differentiation (Lanzuolo, 2012; Collas et al., 2014). Indeed, beyond providing mechanical support to the nucleus, lamins are involved in the regulation of gene expression at various levels

(Shumaker et al., 2006; Scaffidi and Misteli, 2008; Méjat et al., 2009; Lund et al., 2013; McCord et al., 2013). The role of lamin A/C in skeletal myogenesis is suggested by evidence showing that mutations in *LMNA* cause inherited muscle disorders (Zaremba-Czogalla et al., 2011). Although several studies suggest a direct connection between lamin A/C integrity and the transcriptional activity of muscle genes (Favreau et al., 2004; Frock et al., 2006; Cohen et al., 2013; Solovei et al., 2013; Oldenburg et al., 2014), the epigenetic mechanism underlying lamin A/C function during muscle differentiation remains unclear.

The Polycomb group (PcG) of proteins are epigenetic repressors that control a large number of target genes during differentiation (Lanzuolo and Orlando, 2012). The best-characterized PcG protein complexes are Polycomb repressive complex 1 (PRC1) and PRC2. In the nucleus, PcG proteins form microscopically visible foci (Cmarko et al., 2003), and high-throughput data together with microscopy analysis have revealed specific organization of their targets in chromatin loops

Correspondence to Chiara Lanzuolo: chiara.lanzuolo@cnr.it

C. Lanzuolo's present address is Istituto Nazionale Genetica Molecolare Romeo ed Enrica Invernizzi, 20122 Milan, Italy.

Abbreviations used in this paper: 3C, chromosome conformation capture; BX-C, Bithorax complex; ChIP, chromatin immunoprecipitation; colP, coimmunoprecipitation; Ct, cycle threshold; dsRNA, double-strand RNA; GO, gene ontology; HP1, heterochromatin protein 1; KD, knock-down; MB, myoblast; MT, myotube; MyHC, myosin heavy chain; NL, nuclear lamina; PC, Polycomb; PcG, Polycomb group; PDE, partial differential equation; PLA, proximity ligation assay; PRC, Polycomb repressive complex; PRE, Polycomb response element; qPCR, quantitative PCR; RNAPolII, RNA polymerase II; SIM, structured illumination microscopy.

© 2015 Cesarini et al. This article is distributed under the terms of an Attribution-Noncommercial-Share Alike-No Mirror Sites license for the first six months after the publication date (see <http://www.rupress.org/terms>). After six months it is available under a Creative Commons License (Attribution-Noncommercial-Share Alike 3.0 Unported license, as described at <http://creativecommons.org/licenses/by-nc-sa/3.0/>).

Supplemental Material can be found at:  
<http://jcb.rupress.org/content/suppl/2015/11/04/jcb.201504035.DC1.html>  
<http://jcb.rupress.org/content/suppl/2015/11/09/jcb.201504035.DC2.html>  
 Original image data can be found at:  
<http://jcb-dataviewer.rupress.org/jcb/browse/10652>

(Lanzuolo et al., 2007; Bantignies et al., 2011). Interestingly, localization of PRC2 at the nuclear periphery is required for proper muscle differentiation (Wang et al., 2011), and nuclear positioning of the PcG protein–regulated facioscapulohumeral muscular dystrophy locus, whose mutations are responsible for an autosomal dominant neuromuscular disorder, is altered in human *LMNA*-null cells (Masny et al., 2004). Collectively, this evidence suggests that the positioning of PcG proteins in the nucleus and the interplay with lamin A/C are important for PcG protein functions. In line with this hypothesis, lamin A/C-bound DNA domains are enriched in the PcG protein–dependent epigenetic mark H3K27me3 (Lund et al., 2013; Harr et al., 2015). In this paper, we show an evolutionarily conserved cross talk between lamin A/C and PcG proteins that is essential for correct PcG protein repressive functions.

## Results

### Lamin A/C restrains activation of the myogenic program in proliferating myoblasts

As already reported, PcG proteins bind muscle-specific gene promoters in myoblasts (MBs) to prevent premature differentiation (Carette et al., 2004). During myogenic differentiation (Fig. S1 A), total levels of Bmi1 and Ezh2 proteins, belonging to PRC1 and PRC2 complexes, decrease (Fig. S1 B; Carette et al., 2004), and PcG protein binding is lost at muscle-specific loci, resulting in appropriate muscle gene expression. Enforced reduction of *Ezh2* levels by RNAi causes anticipated muscle differentiation in vitro whereas conditional ablation of *Ezh2* in muscle stem (satellite) cells leads to reduced muscle mass (Juan et al., 2011; Woodhouse et al., 2013), resembling the phenotype described for *Lamin A/C*-null mice (Cohen et al., 2013). To unravel the functional relationship between lamin A/C and PcG proteins, depletion experiments using siRNA against *Lamin A/C*, *Ezh2*, or both were performed (Fig. S1 A). To follow muscle differentiation in vitro, we measured the fusion index of confluent MBs and myotubes (MTs) at 1 or 2 d after differentiation (MT1 and MT2, respectively; Fig. 1 A). We confirmed premature muscle differentiation in *Ezh2*-depleted cells. In parallel, we found higher numbers of differentiating cells in both MBs and MT1 upon lamin A/C down-regulation, suggesting anticipation in muscle differentiation. A cumulative effect was not observed after double lamin A/C–*Ezh2* depletion (Fig. 1 A). In contrast, after 48 h in differentiating conditions (MT2), *Ezh2*-depleted cells showed a higher number of myosin heavy chain (MyHC)-positive nuclei, but the fusion index of cells transfected with control or lamin A/C siRNA was comparable (Fig. 1 A, right). We reasoned that this could depend either on a block of differentiation of lamin A/C–depleted MT2 or on the presence of a mixed population of proliferating and differentiating cells.

To discriminate between these two hypotheses, we monitored other parameters of differentiation progression: the length and thickness of MTs and the number of nuclei per fiber. Lamin A/C–depleted MT1 and MT2 were found to be longer and to have a higher number of nuclei per fiber (Fig. S1, C and D), indicating that muscle differentiation proceeded for those cells that started prematurely to fuse. To verify the presence of a proliferating population, we performed a pulse-labeling BrdU assay (Fig. S1 E). As expected, the number of BrdU-positive cells dropped at the onset of muscle differentiation, as cells

exited the cell cycle and started to fuse. However, in *Lamin A/C* knock-down (KD) cells, the number of BrdU-positive cells in MT1 and MT2 was higher than in control-transfected cells, indicating the presence of a proliferating subpopulation of cells. Moreover, lamin A/C–depleted MT1 and MT2 showed comparable rates of BrdU incorporation, suggesting that the proliferating population did not start to differentiate. Collectively, these results reveal that reduction of lamin A/C generates two distinct cell phenotypes: one subpopulation of cells undergoing premature differentiation, and the other failing to exit the cell cycle, thus compromising its differentiation potential. We confirmed our findings on primary muscle satellite cells isolated from single myofibers of C57/BL6 mice (Fig. S1, F and G). To check if lamin A/C function on muscle differentiation was evolutionarily conserved, lamin A/C depletion was also performed in primary human muscle cells (Fig. S1 H). As for mouse cells, a higher number of myosin heavy chain 2- and BrdU-positive cells were found in human MBs treated with lamin A/C siRNA (Fig. S1 I).

In line with myofiber analysis, transcriptional and Western blot analysis of PcG protein–controlled genes involved in early (myogenin, *MyoG*) or late (muscle creatine kinase [*MCK*] and *MyHC*) steps of myogenesis revealed higher levels of transcripts at the onset of differentiation in either *Lamin A/C* or *Ezh2* KD (Fig. 1, B and C), without any influence on cell mortality and proliferation (Fig. S2 A). Double *Ezh2*–*Lamin A/C* depletion did not lead to a cumulative increase of myogenic markers relative to the single *Ezh2* and *Lamin A/C* depletions (Fig. 1 B), as already indicated by MyHC staining (Fig. 1 A), suggesting a common role of the two proteins in the PcG protein repression of target genes. Interestingly, *Desmin*, a gene specific for PcG protein–independent muscles, did not change its expression (Fig. S2 B), and not all PcG protein–regulated genes were found to be altered after *Lamin A/C* depletion (e.g., *NeuroG1* and *HOXD9*), indicating that the perturbation of lamin A/C levels specifically influenced transcription of genes specific for PcG protein–regulated muscles. We also found in *Lamin A/C*-depleted cells aberrant up-regulation of *Pax7* (Fig. S2 B), a PcG protein target normally required for MB proliferation, that could explain the presence of proliferating cells unable to enter muscle differentiation (Fig. S1 E; Relaix et al., 2004; Collins et al., 2005; Lee et al., 2006; Palacios et al., 2010). To further support the notion that lamin A/C affects the transcription level of muscle-specific genes in myogenesis, we perturbed *Lamin A/C* in both primary mouse satellite cells and primary human muscle cells, finding an increase of muscle-specific transcripts (including *Pax7*) in *Lamin A/C*-depleted cells before induction of the differentiation program (Fig. S2, C and D, respectively). Of note, *Lamin A/C* depletion is maintained during differentiation in human primary MBs (Fig. S2 D), as also indicated by the increased expression of myogenic genes in *Lamin A/C*-depleted MTs.

Interestingly, overexpression of human lamin A in C2C12 cells induced an overrepression of muscle genes (Fig. S2 E), mirroring the effect induced by *Lamin A/C* depletion and partially recovering the premature muscle differentiation because of endogenous *Lamin A/C* KD, ruling out that the observed phenotypes were caused by siRNA off-targets. Importantly, *Ezh2* and *Bmi1* protein levels were unaffected by *Lamin A/C* KD in MBs (Fig. S2 F), ruling out the possibility that the lamin-dependent phenotype was caused by lower intracellular levels of PcG proteins. Previous studies on C2C12 cells showed an opposite role of PRC1 and PRC2 complexes in muscle differentiation (Asp et al., 2011), describing aberrant differentiation after

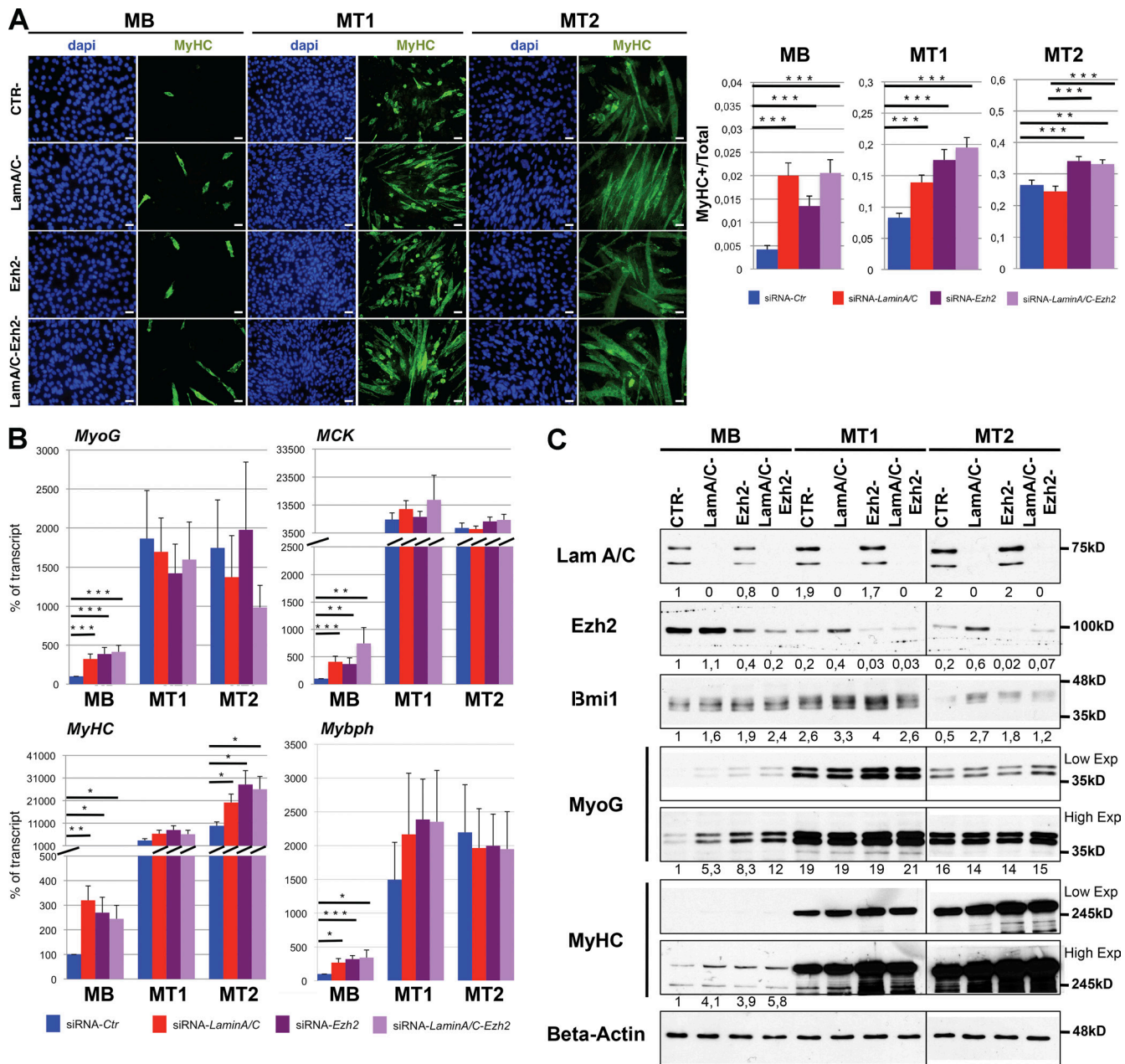


**Figure 1. *Lamin A/C* depletion leads to an anticipation of muscle differentiation in mouse C2C12 cells.** (A, left) Representative images of immunostaining (green: Alexa Fluor 488) for sarcomeric myosin (MyHC) of C2C12 cells transfected with indicated siRNAs. Cells were analyzed as MBs or MTs at MT1 or MT2. Bar, 20  $\mu$ m. (right) Fusion index is calculated as a percentage of nuclei contained in myosin-positive cells with respect to the total number of nuclei.  $n > 5,859$  from three independent experiments. (B) Quantification by real-time PCR of transcript levels relative to GAPDH in C2C12 cells transfected with indicated siRNAs. Data points represent the mean of 10 independent experiments. (C) Western blot of total protein extracts hybridized with indicated antibodies in cells transfected with siRNAs as indicated in A.  $\beta$ -Actin was used as loading control. Numbers indicate quantification of protein bands normalized to  $\beta$ -actin and relative to MB control. Data shown are from a single representative experiment of two repeats. Two-tailed  $t$  test was applied for statistical analysis. SEM is indicated. Statistically relevant differences ( $\alpha = 0.05$ ): \*,  $P < 0.05$ ; \*\*,  $P < 0.01$ ; \*\*\*,  $P < 0.001$ .

depletion of *Bmi1*, a component of the PRC1 complex. We performed *Bmi1* depletion experiments, analyzing the onset of myogenesis. As found with *Ezh2* KD, we observed anticipated muscle differentiation upon *Bmi1* KD that was not enhanced by double *Bmi1*-*Lamin A/C* KD (Fig. S2 G), suggesting that PRC1 and PRC2 complexes share cross talk with *Lamin A/C* and perform common functions at the onset of myogenesis. Finally, to rule out the possibility that the observed phenotype could be a result of broad alterations of NL, we depleted *Lamin B*, one

of the major components of the NL; transcriptional analysis confirmed anticipated muscle gene expression exclusively in *Lamin A/C* KD cells (Fig. S2 H).

#### **Lamin A/C and Ezh2 coregulate muscle-specific genes**

We reasoned that if *Lamin A/C* cooperates functionally with *Ezh2* at the onset of muscle differentiation, they should regulate a common set of target genes. To test this hypothesis, we

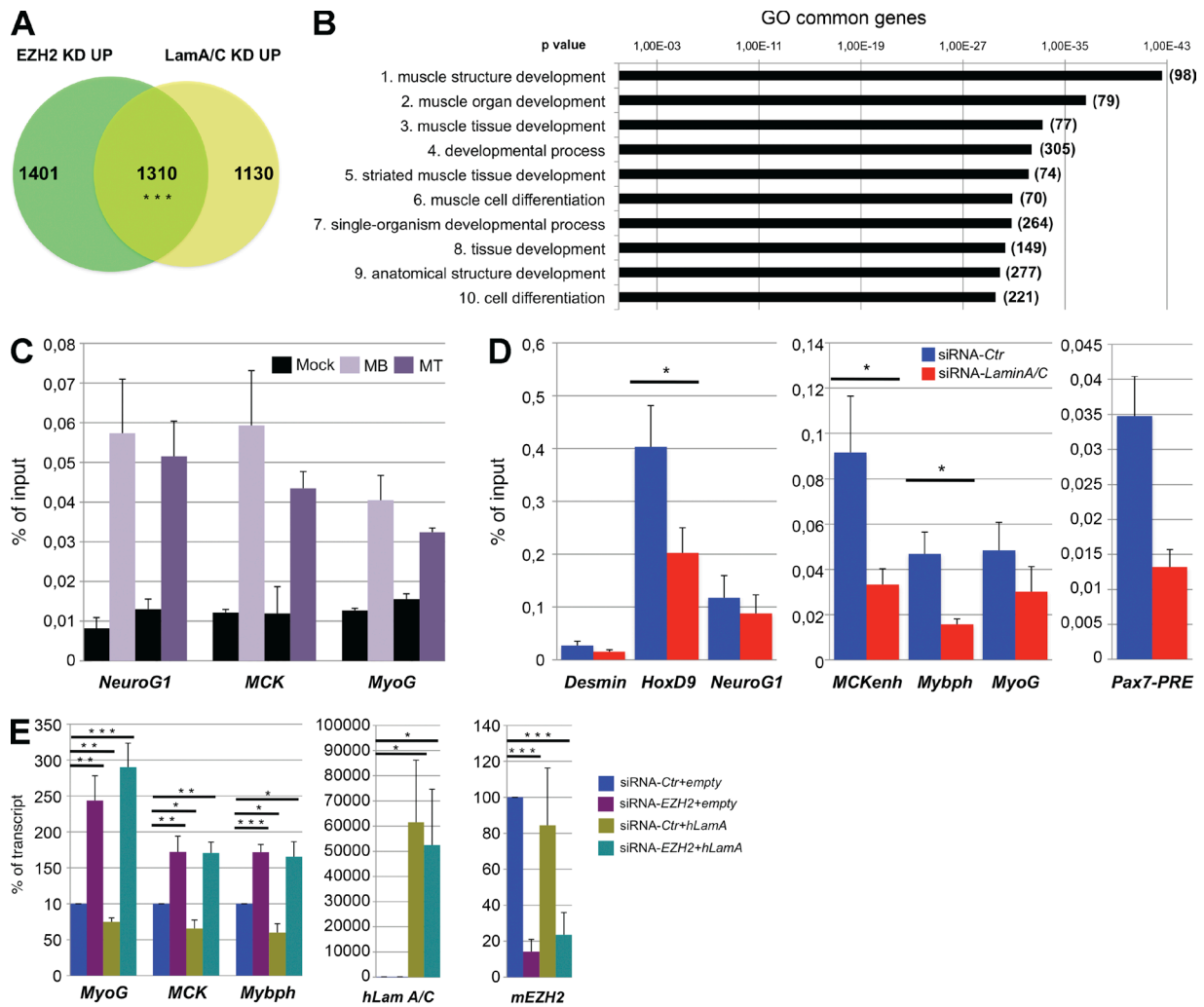


**Figure 2. PcG proteins and lamin A/C coregulate muscle differentiation.** (A) Venn diagram showing intersection between genes up-regulated in *Lamin A/C* or *Ezh2* KD. (B) GO analysis (biological process) of the 1,310 common up-regulated genes showing the top represented GO terms according to P values. The number of genes in each category is reported in brackets. (C) ChIP analyses in MBs or MTs 4 d after differentiation induction (MT4) with antibodies against lamin A/C are presented as a percentage of input chromatin precipitated for indicated regions. Each graph shows the mean of three independent IP reactions on different chromatin preparations. (D) ChIP analyses in C2C12 cells transfected with indicated siRNAs with antibodies against *Ezh2* are presented as a percentage of input chromatin precipitated for indicated regions. Mock enrichment is <0.02% of the input. Data points represent the mean of four independent IP reactions on different chromatin preparations. (E) Quantification by real-time PCR of transcript levels, relative to GAPDH, of indicated genes in C2C12 MBs transfected with a plasmid overexpressing human lamin A or an empty vector as control. C2C12 cells were cotransfected with indicated siRNAs. Data points represent the mean of at least four independent experiments. Two-tailed *t* test was applied for statistical analysis in D and E. SEM is indicated. Hypergeometric test was applied for statistical analysis in A. Statistically relevant differences ( $\alpha = 0.05$ ): \*,  $P < 0.05$ ; \*\*,  $P < 0.01$ ; \*\*\*,  $P < 0.001$ .

performed RNA sequencing in C2C12 cells knocked down for *Lamin A/C*, *Ezh2*, or both. Strikingly, transcriptome analysis revealed that among 2,440 genes up-regulated upon *Lamin A/C* depletion, >50% were similarly affected by *Ezh2* depletion (Fig. 2 A and Tables S1 and S2); the majority of them were also confirmed to be up-regulated in double *Lamin A/C*–*Ezh2* KD (Fig. S3 A and Tables S1 and S2). Gene ontology (GO) analysis of common up-regulated genes indicated a prevalence for subclasses related to muscle development and differentiation (Fig. 2 B and Fig. S3 B). Whereas the transcriptional effects exerted by either lamin A/C or *Ezh2* siRNA are similar, the morphology of C2C12 cells is distinct (Fig. 1 A), *Lamin A/C*–depleted MBs being thinner. To look for possible differential functions, we analyzed the GO of the top 10 categories of genes up-regulated in *Lamin A/C* KD and not in *Ezh2* KD, and vice versa. Indeed, we found that the genes deregulated only

in *Lamin A/C* KD were particularly involved in metabolic processes (Fig. S3 C and Table S3), comprising known players of skeletal muscle atrophy/hypertrophy (i.e., *Akt*, *mTOR*, *Foxo3*; Schiaffino et al., 2013), whereas the GO of genes deregulated only in *Ezh2* KD comprised categories such as control of cell differentiation and development (Fig. S3 D and Table S3), in agreement with the role of PcG protein in controlling the expression of developmental regulators (Lee et al., 2006). This analysis suggests that lamin A/C can regulate, independently of PcG proteins, the transcription of a specific subset of genes implicated in the control of muscle mass.

To investigate the mechanism by which lamin A/C represses muscle genes, we performed chromatin immunoprecipitation (ChIP) analysis with lamin A/C (Fig. 2 C and Fig. S3 E), finding that PcG protein target regions are also occupied by lamin A/C. Interestingly, PcG-regulated muscle gene promoters

showed less binding of lamin A/C upon differentiation (Fig. 2 C), in agreement with studies of PcG proteins, suggesting a coordinated action of both lamin A/C and PcG protein in repressing muscle genes. To further analyze lamin A/C–PcG protein interplay, we monitored PcG protein occupancy on their regulative sequences in siRNA-transfected MBs (Fig. 2 D), finding impaired Ezh2 recruitment on its targets upon lamin A/C depletion. Interestingly, the observed decrease in Ezh2 chromatin binding is not sufficient to transcriptionally activate genes not involved in muscle differentiation, such as *HoxD9* (Fig. S2 B). Finally, to demonstrate that PcG proteins mediate lamin A/C–dependent repression of muscle genes, we depleted *Ezh2* after overexpression of human lamin A in C2C12 cells. We found comparable levels of muscle gene activation in cells treated or not with siRNA against lamin A/C (Fig. 2 E). Thus the overrepression of PcG-regulated muscle genes, observed in the presence of human lamin A (Fig. 2 E), was completely abolished upon *Ezh2* KD, suggesting that lamin A/C represses muscle genes through PRC2. In contrast, the overexpression of human Ezh2 in *Lamin A/C* KD was not sufficient to reduce lamin-dependent premature muscle differentiation (Fig. S3 F), further supporting the idea that the total amount of Ezh2, even at high concentrations, cannot rescue the lamin-dependent phenotype, and that the interplay between lamin A/C and PcG proteins is necessary for correct muscle differentiation.

#### Nuclear compartmentalization of PcG proteins depends on lamin A/C

We analyzed PcG protein nuclear compartmentalization by performing chromatin fractionation experiments in mouse C2C12 cells (Fig. S3 G). Because these were chromatin-bound complexes, we expected PcG proteins to be released from chromatin by DNase treatment. Surprisingly, Western blot analysis revealed that high amounts of Bmi1 and Ezh2 are tightly associated with the lamin A/C–enriched nuclear matrix (Fig. S3 H) in both MBs and MTs. To investigate if the PcG protein enrichment at the nuclear scaffold was dependent on lamin A/C, depletion experiments were performed in C2C12 cells (Fig. 3 A). Using lamin B as control (Fig. S3 I), we found that PcG protein levels significantly decreased in the S4 fraction of both MBs and MTs (Fig. 3 A), although total amounts of PcG proteins did not change upon *Lamin A/C* KD (Fig. S2 F). To measure PcG protein target compartmentalization in control and *Lamin A/C*–depleted cells, we extracted DNA from all the chromatin fractions (S2, S3, and S4). Quantitative PCR (qPCR) analysis, performed on the same DNA quantities, revealed that the distribution of PcG protein and lamin A/C target genes is similarly affected by *Lamin A/C* depletion (Fig. S3 J). In particular, unlike the *Lamin A/C* unbound region (*Sun1p0*; Fig. S3 E), a significant proportion of *Lamin A/C*–bound genes, including PcG protein targets, are reduced in the matrix fraction and enriched in the DNase-sensitive fraction (Fig. S3 J), further confirming a specific role of lamin A/C in PcG protein intranuclear compartmentalization. We thus checked, by performing reciprocal coimmunoprecipitation (coIP) experiments, if lamin A/C could interact with PcG proteins (Fig. S3 K). We found that endogenous lamin A/C weakly interacts with members of both PRC1 and PRC2. To confirm the occurrence of an interaction between lamin A/C and PcG proteins, we used a proximity ligation assay (PLA), which permits the detection of transient interactions occurring between two proteins located in close proximity (<30 nm) within the nuclear space of intact cells (Fredriksson et al.,

2002). In particular, by using different combinations of antibodies against lamin A, lamin B, Ezh2, and Bmi1 in C2C12 cells, we demonstrated that lamin A, but not lamin B, specifically interacts with PcG proteins in the nucleus (Fig. 3 B). As a positive control, we performed lamin A/B PLA, finding dots at the nuclear periphery where lamin A and B colocalize (Moir et al., 2000).

To further characterize the nature of lamin A–PcG protein interactions within the nuclear volume, we analyzed PcG protein intranuclear localization by 3D structured illumination microscopy (SIM; superresolution microscopy). We noticed that lamin A/C forms structures in the nucleoplasm that surround or are in close proximity to PcG protein foci (Fig. 4 A). In fact, nucleus sections show a precise interlock of green (Bmi1) and red (lamin A/C) signals, suggesting an interdependent distribution of the two proteins. Thus we measured the minimum distances of lamin A/C (Fig. 4 B) or lamin B (Fig. 4, C and D) signals from adjacent PcG protein foci in the 3D reconstructed nuclei, finding that although a significant proportion of lamin A/C is found proximal to PRC1 molecules (Fig. 4 B), lamin B is always located at a distance from PcG foci (Fig. 4 D). Distribution of distances measured between lamin B and lamin A/C (Fig. 4, E and F), which have been described to form separate, but interacting, stable meshwork in the lamina (Shimi et al., 2008), resembles the association we have shown here that occurs between PcG protein and lamin A/C. As a control, we analyzed RNA polymerase II (RNAPolII), which is able to form aggregates in the nucleus called transcriptional factories (Fig. 4, G and H). The broader distribution of distances between RNAPolII and lamin A/C suggests that fewer RNAPolII molecules are found in proximity to lamin A/C compared with PcG.

#### Lamin A/C depletion leads to PcG protein intranuclear diffusion

To investigate the mechanism by which lamin A/C regulates PcG protein nuclear distribution, we analyzed PcG protein foci organization in C2C12 MBs transfected with siRNA against lamin A/C or control (Fig. S4 A). Lower fluorescence signals of Ezh2 and Bmi1 were found in *Lamin A/C*–depleted confluent MBs. Because Ezh2 and Bmi1 total protein levels were unaltered upon *Lamin A/C* depletion (Fig. S2 F), this result suggests intranuclear diffusion of PcG proteins in the absence of lamin A/C. In particular, we noticed that misshapen nuclei defective of lamin A/C (white arrows) showed minimal levels of PcG protein staining. This evidence prompted us to further investigate the role of lamin A/C in the conformation and localization of PcG protein foci (Fig. 5 A). To speed up image analysis and automatically select PcG foci, we developed specific software relying on two novel image segmentation algorithms (see Image analysis) that can capture PcG foci areas isolated from nucleus regions (Fig. 5 B). The first algorithm separates nucleus regions from background, whereas the second algorithm separates PcG bodies from nuclei. The first algorithm gave accurate results for our purpose, which was to preserve the integrity of nucleus regions. We compared the second algorithm with other well known thresholding algorithms (Sezgin and Sankur, 2004), achieving more accurate segmentation results, as shown in Fig. S4 B. We validated our software by performing PcG foci analyses on *Bmi1* KD cells (Fig. S4 C), finding few PcG foci in the absence of Bmi1.

By analyzing the number and size of PcG foci, we observed that the *Lamin A/C*–depleted population exhibits a higher number of cells with fewer (Fig. 5 C) and smaller (Fig. 5 D) PcG foci compared with control cells. Similar results were obtained

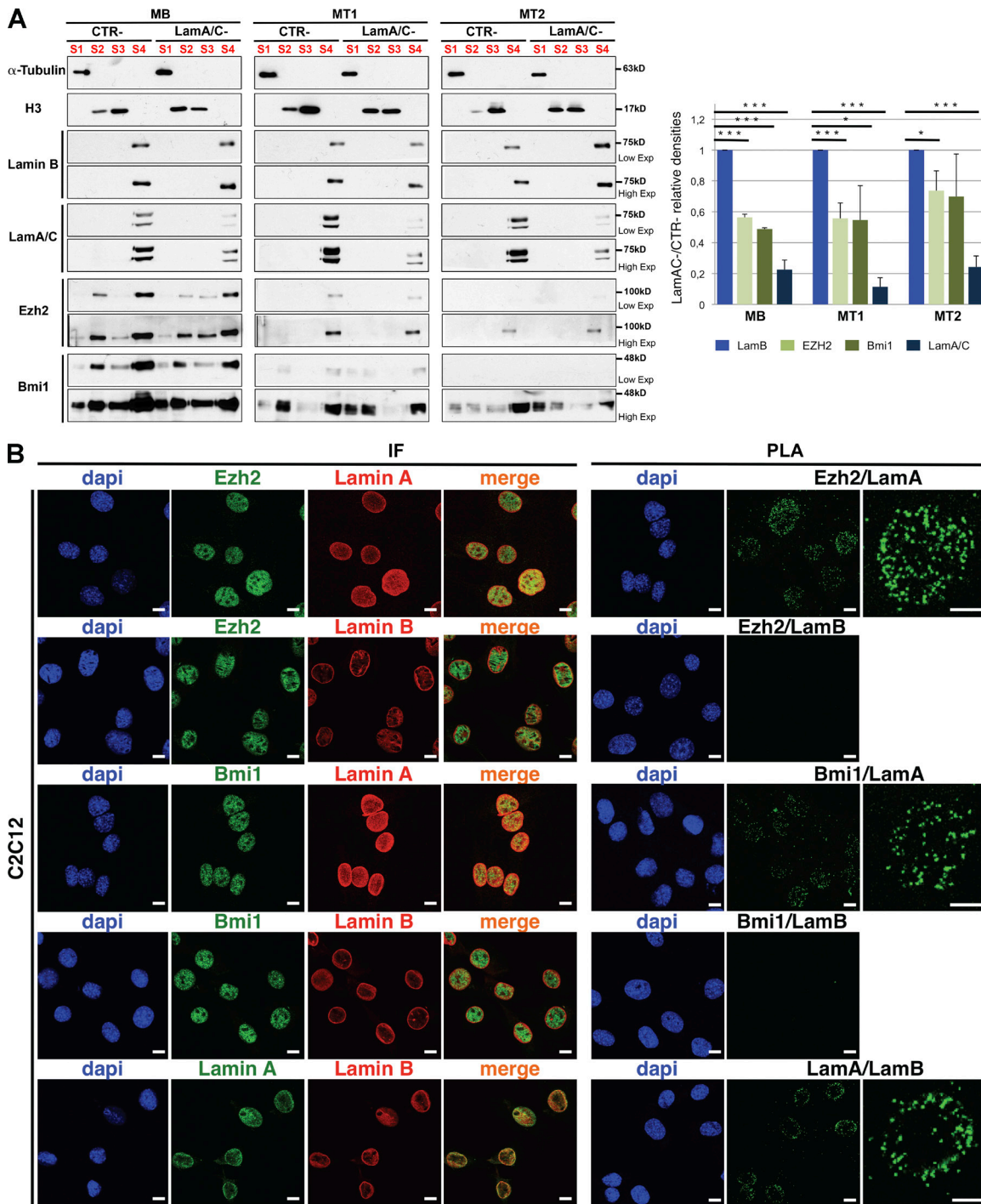


**Figure 3. PcG proteins and lamin A/C interact endogenously.** (A, left) Chromatin fractionation experiments of C2C12 cells transfected with indicated siRNAs and collected as MBs or MTs at MT1 or MT2. Sequential protein extractions were performed to isolate soluble proteins (S1 fraction), DNase-sensitive proteins (S2 fraction), DNase-resistant proteins (S3 fraction), and nuclear matrix-associated proteins (S4 fraction). Equal amounts of each fraction were immunoblotted and hybridized with indicated antibodies. Loading controls:  $\alpha$ -tubulin (S1), histone H3 (S2 and S3), and lamin B (S4). (right) Quantification of indicated proteins in S4 fraction, normalized to lamin B. Data points represent the mean of at least three biological replicates. Two-tailed *t* test was applied for statistical analysis. SEM is indicated. Statistically relevant differences ( $\alpha = 0.05$ ): \*,  $P < 0.05$ ; \*\*\*,  $P < 0.001$ . (B) Representative confocal microscopy images of C2C12 MBs RNA immunostained using the indicated antibodies (green, Alexa Fluor 488; red, Alexa Fluor 594) and DAPI (left), with relative PLA experiments (right). Bar, 10  $\mu$ m. Each fluorescent dot represents the colocalization between the indicated antibodies. Data shown are from a single representative experiment of two repeats. IF, immunofluorescence.

by immunostaining C2C12 cells with antibodies against Ezh2, indicating that lamin A/C affects foci organization of PcG proteins belonging to both PRC1 and PRC2 (Fig. S4 D). Importantly, analysis of heterochromatin protein 1 (HP1) foci in

Lamin A/C-depleted cells did not show the same effect (Fig. S4 E), and analysis of PcG foci after Lamin B depletion did not show a decrease in number or area of PcG foci (Fig. S4 F), indicating a specific role of lamin A/C in PcG foci maintenance

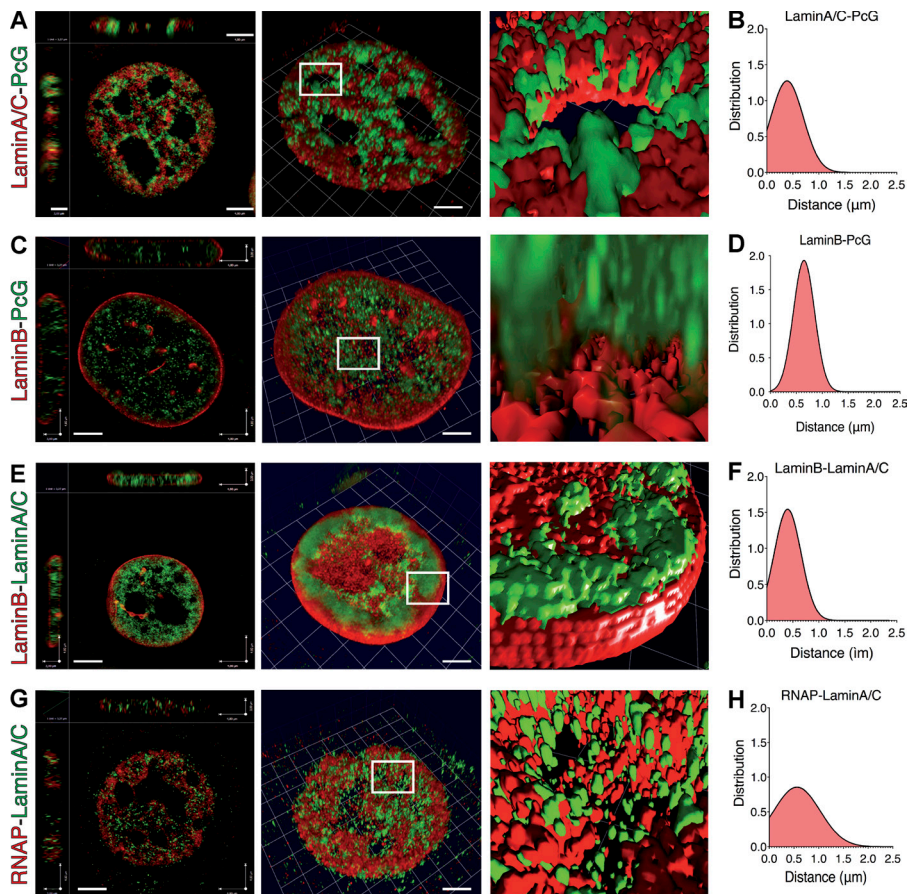


**Figure 4. Lamin A/C surrounds PcG foci.** (A, C, E, and G, left) Mid z-section and the relative orthogonal projections of C2C12 nuclei stained for lamin A/C and Bmi1 (A); lamin B and Ring1b (C); lamin B and lamin A/C (E); and RNAPolII and lamin A/C (G) and acquired with N-SIM superresolution system. Bar, 4  $\mu$ m. middle: 3D reconstruction of the entire nuclear volume. Bar, 4  $\mu$ m. (right) 3D surface rendering of both signals within the nuclear volume. The image represents a magnification of the squared image shown in the middle. (B, D, F, and H) Protein foci of two nuclei from a single experiment were analyzed: distribution of the relative distances in the 3D nuclei volumes measured as the minimum distances occurring between lamin A/C and Bmi1 (PcG foci  $n = 7,243$ ; B); lamin B and Ring1b (PcG foci  $n = 7,054$ ; D); lamin B and lamin A/C (lamin spots,  $n = 4,837$ ; F); and RNAPolII and lamin A/C (RNAPolII spots,  $n = 5,228$ ; H). Green, Alexa Fluor 488; red, Alexa Fluor 594.

and ruling out the possibility that the observed changes could be caused by general defects in NL or heterochromatin compaction. To further characterize PcG foci in *Lamin A/C*-depleted cells, we estimated their volume by assembling the segmented image stacks and using the 3D Object Counter ImageJ plugin (Fig. 5 E; Bolte and Cordelières, 2006), finding even more significant differences in class distributions. To confirm these data, we used muscle satellite cells isolated from the *Lamin  $\Delta 8-11$*  knockout mouse (Sullivan et al., 1999; Jahn et al., 2012), showing fewer and smaller PcG foci in the mutant cells compared with satellite cells derived from their wild-type littermates (Fig. 5 F).

To understand whether *Lamin A/C* depletion affects the correct assembly of Polycomb (PC) complexes, we used the PLA assay between two components of PRC1 (Bmi1 and Ring1b; Fig. 6 A). *Bmi1* depletion was also performed to validate the results. Intriguingly, we observed an increased number of “blobs” in *Lamin A/C*-depleted cells compared with control-transfected cells (Fig. 6 B). These data indicate that *Lamin A/C* depletion does not alter PRC1 complex assembly, but suggests rather that upon *Lamin A/C* KD, PRC1 complexes are more diffused and no longer centered in single PcG foci. To further analyze the effect of *Lamin A/C* depletion on PcG protein nuclear distribution, we performed EM analysis with Bmi1 antibodies (Fig. 6 C). In line with previous evidence (Satijn et al., 1997; Cmarko et al., 2003; Šmigová et al., 2011), although we could not visualize PcG foci by EM, we found a specific signal for Bmi1 that localizes in discrete nuclear areas. In the nucleoplasm, Bmi1 localized at the nucleoli borders, where nucleoplasmic lamina-associated domains were also found (Kind and van Steensel, 2014), and at the euchromatin-heterochromatin junctions.

Strikingly, in *Lamin A/C*-depleted cells, Bmi1-associated particles lose their proper localization, spreading through the whole nucleus, including nucleoli interiors, euchromatin, and heterochromatin (Fig. 6 C, right panels), suggesting an aberrant broad diffusion of the Bmi1 protein. Importantly, EM images did not show decondensation of heterochromatin in *Lamin A/C*-depleted cells (Fig. 6 C), indicating that the observed *Lamin A/C* KD-dependent phenotypes are not caused by broad alterations of chromatin structures from a damaged nuclear scaffold.

#### Functional interaction between lamin A/C and PcG proteins is evolutionarily conserved

To test whether the functional relationship between PcG protein and A-type lamins is conserved throughout evolution, we investigated their interplay in *Drosophila melanogaster*, a model system in which PcG protein functions have been extensively characterized (Delest et al., 2012). In *Drosophila*, there are two lamin genes: *lamin C* and *lamin Dm0*, which have been classed as A- and B-type lamins, respectively, on the basis of their expression patterns (Gruenbaum et al., 1988; Riemer and Weber, 1994). Flies lacking A-type lamin or ectopically expressing a mutated form of human lamin A show nuclear envelope defects similar to those observed in human laminopathies (Muñoz-Alarcón et al., 2007; Beard et al., 2008; Dialynas et al., 2012; Zwerger et al., 2013), suggesting an evolutionarily conserved function for A-type lamin proteins (Schulze et al., 2009). We used *Drosophila* embryonic S2 cells as a model, in which the homeotic genes of Bithorax complex (BX-C) are silenced by PcG proteins (Lanzuolo et al., 2007; Fig. S5 A), and we investigated the role

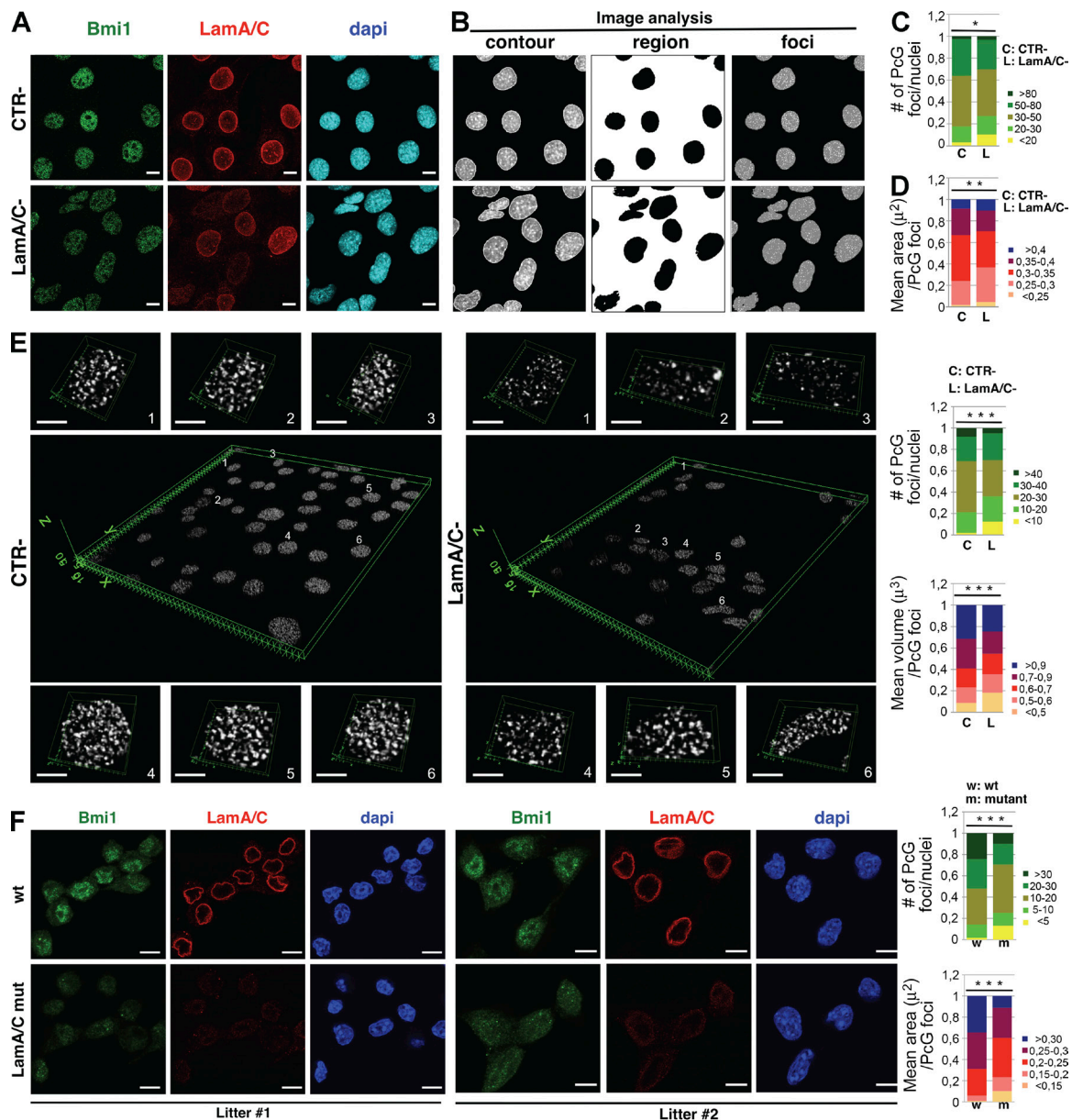


**Figure 5. PcG foci integrity is dependent on lamin A/C.** (A) Representative confocal microscopy images of C2C12 MBs transfected with indicated siRNAs. (B) Contour of nuclei, selected regions, and PcG foci in segmentation analysis. Segmentation was performed as indicated in Image analysis. Bar, 10  $\mu\text{m}$ . (C and D) 2D analysis of PcG foci of C2C12 MBs transfected as indicated in A. (C) Distribution of number of PcG foci per nucleus among the cellular population. (D) Distribution of PcG foci area (measured in  $\mu\text{m}^2$ ).  $n > 244$  from three independent experiments. (E) 3D reconstruction of single nuclei from C2C12 MBs transfected as indicated in A. Bar, 10  $\mu\text{m}$ . right: 3D analysis of PcG foci. Distribution of number of PcG foci (top) and PcG foci volumes (bottom; measured in  $\mu\text{m}^3$ ) among the cellular population.  $n > 316$  from three independent experiments. (F) 2D analysis of PcG foci of satellite myoblast cells extracted by FACS from homozygous Lamin  $\Delta 8-11$  mice (LamA/C mut) and their wild-type (wt) littermates. Bar, 10  $\mu\text{m}$ . (right) Distribution of number of PcG foci per nucleus (top) and PcG foci area (bottom; measured in  $\mu\text{m}^2$ ) among the cellular population.  $n > 100$  from two independent experiments. Mann-Whitney two-tailed test was applied for statistical analysis. Statistically relevant differences ( $\alpha = 0.05$ ): \*,  $P < 0.05$ ; \*\*,  $P < 0.01$ ; \*\*\*,  $P < 0.001$ . Green, Alexa Fluor 488; red, Alexa Fluor 594.

of lamin C in the regulation of PcG protein-dependent epigenetic signatures through RNAi experiments. As already found in mouse C2C12 cells, although PC and  $E(z)$  total levels were not altered (Fig. 7 A and Fig. S5 B), chromatin fractionation experiments in *Lamin C*-depleted cells revealed that the amount of PC and  $E(z)$  consistently decreased in matrix fraction S4 (Fig. 7 B), further indicating that the role of lamin A/C in favoring PcG protein localization at the nuclear matrix is evolutionarily conserved. Of note, none of the observed differences were influenced by the growth potential or mortality of depleted cells (Fig. S5 C).

To test if PcG protein recruitment on chromatin was influenced by *Lamin C* depletion, we performed CHIP analysis on the minimal promoters of *Ubx* and *abdA* genes and their regulatory Polycomb response elements (PREs), *bxl* and *mcp*, finding that PC binding was significantly reduced on PREs (Fig. 7 C). To understand whether the observed differences of PC binding were limited to minimal PcG protein binding sites or spread along the chromatin fiber, we extended the analysis to regions surrounding PREs and promoters. As shown in Fig. S5 D, we found a decrease of PC only on and around

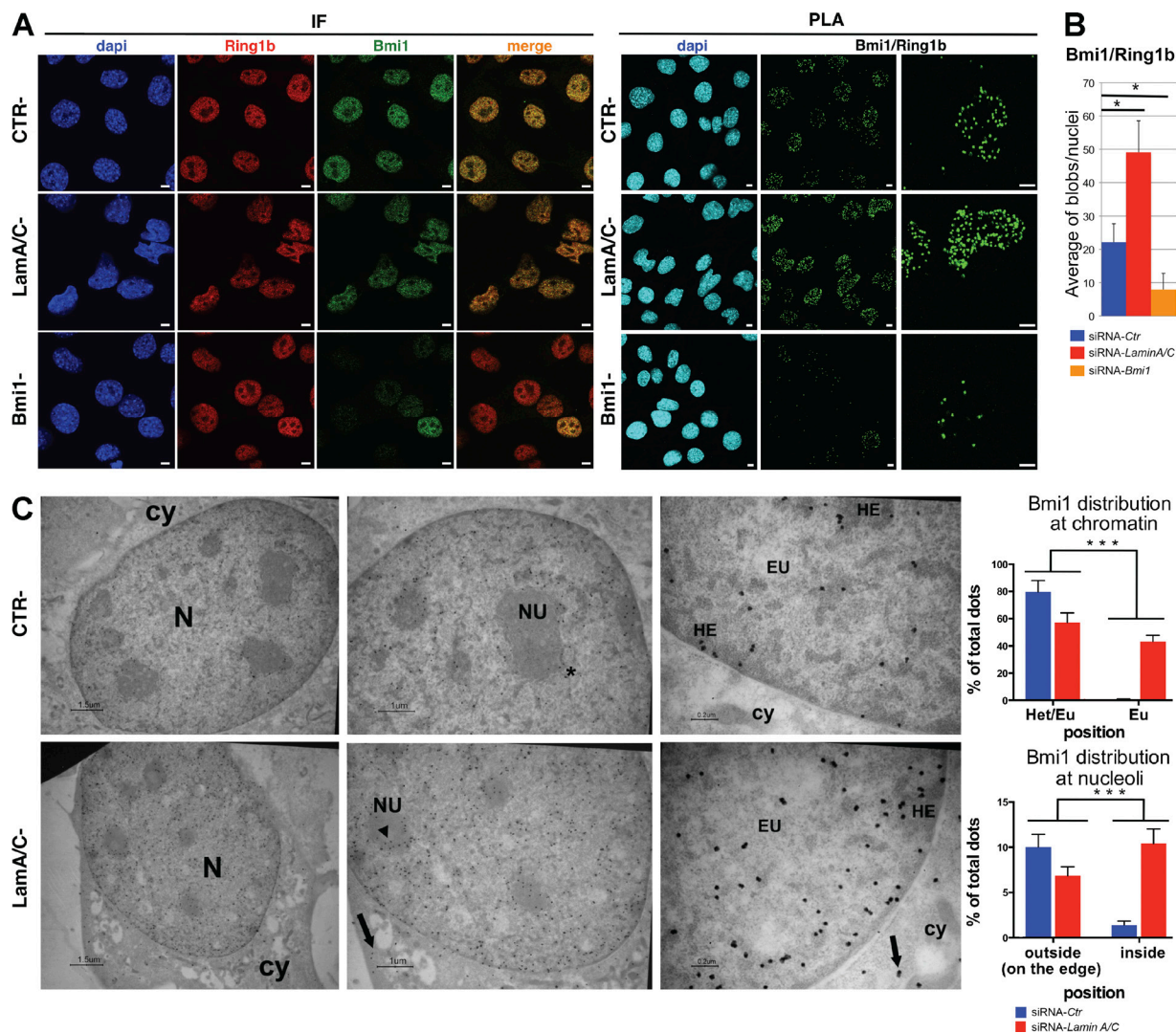


**Figure 6. Lamin A/C depletion leads to Bmi1 delocalization and PRC intranuclear diffusion.** (A) Representative confocal microscopy images of C2C12 MBs transfected with indicated siRNAs and immunostained using Bmi1, Ring1b antibodies, and DAPI (left), with the relative PLA experiments (right). Bar, 10  $\mu$ m. Each fluorescent dot represents the colocalization of Bmi1 and Ring1b within the cells (B).  $n > 191$  from four independent experiments. Two-tailed  $t$  test was applied for statistical analysis. SEM is indicated. Green, Alexa Fluor 488; red, Alexa Fluor 594. (C, left) Representative EM images of anti-Bmi1 immunogold labeling in C2C12 MBs transfected with indicated siRNAs (three different magnifications are shown). In the control, anti-Bmi1 antibody is specifically localized to condensed regions of heterochromatin (HE), whereas euchromatic regions (EU) are unlabeled. The gold particles are present at the border of the nucleolus (\*). In *lamin A/C*-depleted C2C12 MBs, a significant increase of the labeling is diffused in the nucleus over HE and EU regions. Intranucleolar label (arrowheads) is also present. A few gold particles are randomly scattered in the cytoplasm (arrows). (right) Quantification of Bmi1 dot distribution in C2C12 cells transfected with siRNAs against *lamin A/C* or control. (top) Percentage of dots localized in the junction between heterochromatin and euchromatin (Het/Eu) or aberrantly localized in euchromatin (Eu). (bottom) Percentage of dots localized on the edge of nucleoli (outside) or aberrantly localized in nucleoli (inside) are shown.  $n > 84$  from two independent experiments. Two-way analysis of variance was applied for statistical analysis. Statistically relevant differences ( $\alpha = 0.05$ ): \*,  $P < 0.05$ ; \*\*\*,  $P < 0.001$ . N, nucleus; NU, nucleolus; cy, cytoplasm; IF, immunofluorescence.

PREs. Analysis of BX-C homeotic genes displayed unaltered transcriptional levels after *Lamin C* depletion (Fig. S5 E), in line with what we observed for the mammalian homeotic gene *HoxD9* (Fig. S2 B). We thus monitored the dynamics of homeotic gene reactivation after PC reduction in the absence of lamin C. We found that in *Pc-lamin C* double mutants, homeotic gene de-repression was consistently higher compared with single *Pc* depletion (Fig. 7 D and Fig. S5, F and G). Notably, *bw*, a heterochromatic gene not controlled by PcG proteins (Paro and Zink, 1993), was not reactivated by *Lamin C* reduction (Fig. 7 D).

To further characterize PcG protein intranuclear distribution in *Lamin C*-depleted cells, we performed PcG foci analysis

on double-strand RNA (dsRNA)-transfected cells (Fig. S5 H). As observed in C2C12 cells, *Lamin C*-depleted S2 cells exhibited few and smaller PcG foci and 3D nuclei reconstruction further confirmed this finding (Fig. 7 E). In *Drosophila*, PcG proteins mediate DNA-DNA interactions among their targets, including PREs and core promoters, generating the formation of chromosome loops (Lanzuolo et al., 2007; Bantignies et al., 2011; Tolhuis et al., 2011). To investigate whether PcG protein-mediated BX-C higher-order structures were affected by *Lamin C* depletion, we used chromosome conformation capture (3C) analysis, monitoring PRE promoters and PRE-*PRE* interactions. Comparison of cross-linking frequencies in depleted versus control cells revealed that, although the

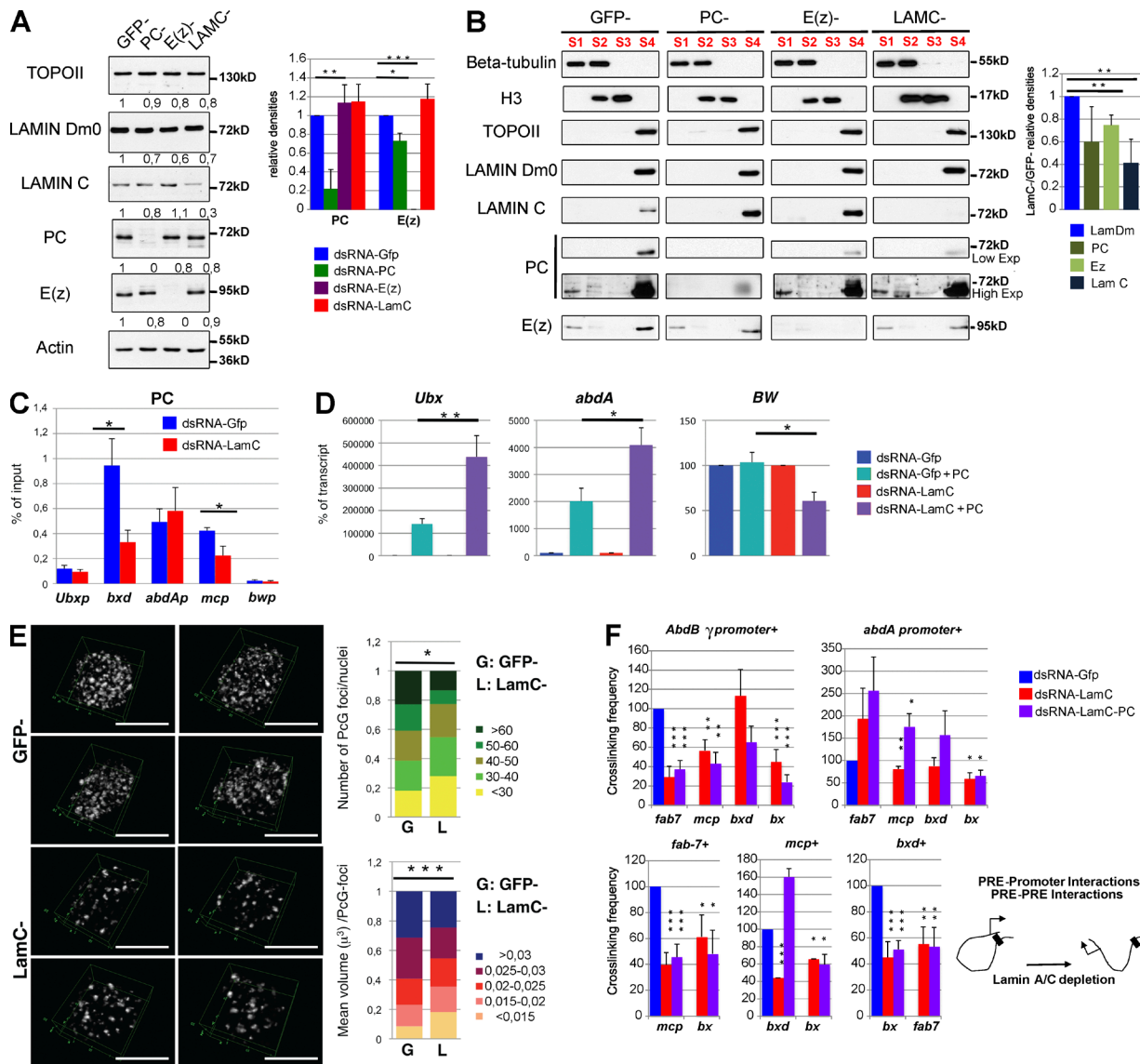


**Figure 7. *Drosophila* lamin C is necessary for PcG protein intranuclear localization and function.** (A) Western blot of total protein extracts hybridized with indicated antibodies in cells transfected with indicated dsRNAs.  $\beta$ -Actin was used as loading control. Topoisomerase II and lamin Dm0 were used as controls to verify the integrity of nuclear matrix. Numbers indicate quantification of protein bands normalized to  $\beta$ -actin and relative to GFP. Data shown are from a single representative experiment of five repeats. The graph indicates quantifications of protein bands normalized to  $\beta$ -actin and relative to MB control. (B, left) Chromatin fractionation experiments of cells transfected as indicated in A. Equal amounts of each fraction were immunoblotted and hybridized with indicated antibodies. Positive controls:  $\beta$ -tubulin (S1, S2), histone H3 (S2, S3), and lamin Dm0 and topoisomerase II (S4). (right) Quantification of indicated proteins in S4 fraction, normalized to lamin Dm0. Data points represent the mean of at least two biological replicates. (C) ChIP analyses with antibodies against PC are presented as a percentage of input chromatin precipitated for the indicated region. Mock enrichment is  $<0.003\%$  of the input. As negative control, we used the promoter region of *brown* (*bw*) that is repressed in S2 but is not under the control of PcG proteins (Paro and Zink, 1993). Data points represent the mean of five independent IP reactions on different chromatin preparations. (D) Quantification by real time-PCR of transcript levels, relative to GAPDH, of homeotic genes in cells transfected with indicated dsRNAs. Data points represent the mean of six independent experiments. (E, left) 3D reconstruction of single nuclei from S2 cells transfected with indicated dsRNAs and immunostained using PC antibodies. Bar, 10  $\mu$ m. (right) Distribution of number of PcG protein foci per nucleus (top) and PcG foci volume (bottom; measured in  $\mu$ m<sup>3</sup>) among the cellular population.  $n > 75$  from three independent experiments. (F) 3C experiments in cells transfected with indicated dsRNAs. Cross-linking frequencies, normalized to the GFP control, between the two homeotic promoters (*AbdB*  $\gamma$  promoter+ and *abdA* promoter+) and BX-C PREs or between PRE and PRE are shown. Data points represent the mean of at least eight independent biological replicates. Two-tailed *t* test was applied for statistical analysis in A, B, C, D, and F. SEM is indicated. Mann-Whitney two-tailed test was applied for statistical analysis in E. Statistically relevant differences ( $\alpha = 0.05$ ): \*,  $P < 0.05$ ; \*\*,  $P < 0.01$ ; \*\*\*,  $P < 0.001$ .

overall BX-C structure was maintained, several PcG protein-dependent DNA-DNA interactions were reduced in the absence of lamin C (Fig. 7 F). Of note, 3C analysis in double *Pc-lamin C* KD cells gave rise to comparable results relative to single *Lamin C* KD, suggesting that lamin C-dependent impairment of BX-C higher-order structures is not exacerbated by lack of *Pc* (Fig. 7 F).

## Discussion

PcG proteins are epigenetic factors that, by forming aggregates in the nucleus and mediating higher-order chromosome looping, ensure the correct transcriptional repression of genes involved in development and differentiation processes (Bantignies and Cavalli, 2011; Lanzaolo and Orlando, 2012). Here, we

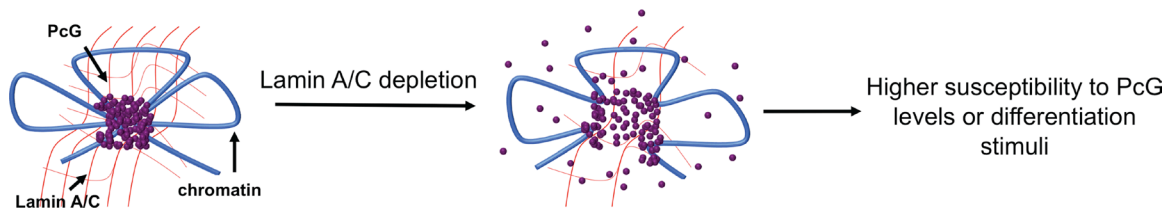


Figure 8. **Lamin A/C sustains PcG protein intranuclear architecture.** Reduction of lamin A/C levels determines an erosion of PcG foci caused by PcG protein dispersion. This is accompanied by a relaxation of PcG-mediated higher-order chromatin structure that acquires a conformation more prone to transcriptional reactivation.

uncover a novel conserved functional regulator of PcG proteins: the structural component of the nucleus lamin A/C. We found that a subset of lamin A/C molecules interact with PcG proteins (Fig. 3 B), and that this is necessary for the conserved nuclear compartmentalization of PcG proteins (Figs. 3 A, 5, 6, and 7, B and E) and targets (Fig. S3 J). Mature lamin A is found not only at the nuclear periphery, but also within the nucleoplasm, where it exists as a detergent-soluble pool (Hozák et al., 1995; Kolb et al., 2011). In our study, we found PcG protein foci localized at the nuclear interior in close proximity to lamin A/C (Figs. 3 B, 4, and 5) and mostly excluded from peripheral locations where lamin B is present. This suggests that the association of PcG proteins with lamin A/C takes place in the nucleoplasm, as indicated by PLA experiments (Fig. 3 B). We then demonstrated, by 2D and 3D immunofluorescence, that alteration of lamin A/C causes PcG foci erosion (Figs. 5 and 7E and Figs. S4 D and S5 H). In line with these data, PLA and EM experiments revealed that even if PRC1 subunits are still able to interact with each other after *Lamin A/C* depletion, the complex they form is not aggregating anymore in bodies and is aberrantly localized on the chromatin (Fig. 6). Super-resolution microscopy further suggested that the correct compaction and localization of PcG foci requires lamin A/C, showing a nonrandom distribution of the two proteins, with PcG foci embedded in the nucleoplasmic lamin A/C structures (Fig. 4). Functionally, in parallel with PcG foci erosion, we observed a reduction of PcG protein chromatin binding upon *Lamin A/C* depletion, in both *Drosophila* and mammals (Figs. 2 D and 7 C), that led to transcriptional activation of some target genes (Fig. 1 B and Fig. S2, B–D). Not all PcG protein targets were de-repressed after lamin A/C reduction; indeed, *Hox* transcription was unaffected by *Lamin A/C* depletion in both mammals and *Drosophila* model systems (Figs. S2 B and S5 E). Nonetheless, PcG protein targets that remain repressed after *Lamin A/C* depletion acquire an epigenetic state more susceptible to PcG protein fluctuations (Fig. 7 D). Accordingly, 3C experiments showed that A-type lamin depletion determines impairment of PcG-dependent genomic association at the *Hox* cluster (Fig. 7 F) that leads to instability of PcG protein transcriptional repression (Fig. 7 D). Interestingly, slackening of *Lamin C* KD-dependent BX-C higher-order structures is not exacerbated by lack of PC. Previous 3C studies on BX-C have shown that depletion of PC or single PcG protein subunits only marginally impairs BX-C 3D structure and that PcG proteins exhibit a synergistic role in the maintenance of higher-order structures (Lanzuolo et al., 2007; Lo Sardo et al., 2013). In line with the current model, our findings suggest that lamin C is important for the strength or maintenance of PcG protein-dependent higher-order chromatin structures controlling multiple PcG protein subunits (Figs. 7 F and 8).

It has been previously shown in worms that in a lamin-defective background, muscle promoters do not relocalize from the nuclear periphery to a more internal location in differentiating muscle cells (Mattout et al., 2011). Accordingly, here we report an epigenetic role for lamin A/C in the regulation of muscle differentiation, finding that *Lamin A/C* depletion accelerates the myogenic program (Fig. 1 A and Fig. S1, G and I). This is dependent on premature transcription of PcG protein-regulated muscle genes (Fig. 1 B and Fig. S2, C and D) because of a detachment of Ezh2 from chromatin (Fig. 2 D). Transcriptome analysis corroborated these findings, showing an extended overlap between *Lamin A/C* and *Ezh2* KD up-regulated genes (Fig. 2 A), mostly involved in muscle differentiation (Fig. 2 B). This evidence strongly suggests that lamin A/C and Ezh2 functionally cooperate to silence common targets involved in myogenic differentiation, as also confirmed by ChIP analysis (Fig. 2 C). In line with our work, genome-wide studies indicate that depletion of *Lamin A/C* in adipocytes results in an increased proportion of genes enriched in H3K4me3, independently of their association with *Lamin A/C*. Those authors suggested that lamin A/C may compete with the Trithorax group proteins (Lund et al., 2013; Collas et al., 2014), the physiological antagonists of PcG proteins, responsible for H3K4me3 deposition (Schuettengruber et al., 2011). Our findings support this hypothesis, suggesting that in the absence of lamin A/C, the activity of Trithorax group proteins may be favored by the destabilization of PcG protein structures.

Prior experiments, performed in either satellite cells from *Lamin A/C*-null mice or *Lamin A/C*-depleted MBs, described a defect in muscle differentiation and proposed lamin A/C as a positive regulator of myogenesis (Frock et al., 2006; Solovei et al., 2013). In other conditions, however, satellite cells from *Lamin A/C*-null mice showed a normal ability to differentiate and form MBs, suggesting rather a defect in cell proliferation (Melcon et al., 2006; Cohen et al., 2013). The discrepancy among observed *Lamin A/C* mutant phenotypes could be ascribed to the different time windows investigated by different authors and by distinct methodology to interfere with *Lamin A/C* functions. Here we show that reduced levels of lamin A/C lead to an anticipated onset of muscle differentiation (Fig. 1 A), accompanied by the appearance of a subpopulation of cells that fail to enter the myogenic program (Fig. S1, E, G, and I). In the mouse model, coexistence of the two populations could lead to a general impairment of muscle differentiation at later stages.

Altogether, our findings unveil a novel role of lamin A/C in mediating PcG protein functions at various levels, by regulating PcG protein subnuclear localization and assisting PcG protein chromatin engagement and formation of higher-order structures, ultimately enforcing PcG protein-mediated transcriptional repression (Fig. 8).

## Materials and methods

### Cell cultures

C2C12 mouse myoblasts cells (ATCC) were cultured in DMEM supplemented with 10% FBS (Euroclone). Differentiation was induced when cells reached ~80% confluence using DMEM containing 2% horse serum (Euroclone). Muscle satellite cells were isolated from 2-mo-old wild-type C57BL/6J or 3-wk-old Lamin  $\Delta 8-11$  homozygous mice. Single muscle fibers from adult mice were isolated by standard procedures (Rosenblatt et al., 1995). In brief, hindlimb muscles were digested with collagenase, and single myofibers were cultured in growth medium 1 (DMEM supplemented with 10% horse serum [Gibco], 0.5% chick embryo extract [MP Biomedicals], and penicillin-streptomycin [Gibco]) and plated on matrigel-coated dishes (1 mg/ml ECM gel; Sigma-Aldrich) for satellite cell culture. Three days later, the fibers were removed and the medium was replaced with proliferation medium (growth medium 2: 20% FBS, 10% horse serum, and 1% chick embryo extract in DMEM). After 3 d, the medium was replaced with differentiation medium (2% horse serum and 0.5% chick embryo extract in DMEM) for 6 d.

Human primary myoblasts from healthy donors were obtained from M. Mora, Telethon BioBank, C. Besta Institute, Milan, Italy. Muscle cells were cultured in DMEM supplemented with proliferation medium (20% FBS, 10 mg/ml human recombinant insulin [Sigma-Aldrich], 25 ng/ml bFGF [Tebu-Bio], and 10 ng/ml EGF [Tebu-Bio]) and induced to differentiate in DMEM supplemented with 2% horse serum (differentiation medium). *Drosophila* embryonic S2 cells were grown at 25°C in serum-free insect culture medium (HyQ SFX; Hyclone) supplemented with penicillin/streptomycin.

### Strains

The generation of *Lmna*<sup>-/-</sup> mice has been described (Sullivan et al., 1999). In brief, to produce the targeting vector, an NsiI–BamHI fragment was deleted, removing exon 8 to part of 11, and replaced with a neomycin resistance cassette. Further studies revealed that the truncated *Lmna* mutant lamin A $\Delta 8-11$  persists in the *Lmna*<sup>-/-</sup> mouse line, which has previously been considered as completely deficient for A-type lamins (Jahn et al., 2012). Thus the Lamin  $\Delta 8-11$  knockout mouse used in this study presents a deletion of the last exons of the gene, leading to the production of a truncated form of lamin A, deleted from the C-terminal domain.

### Antibodies

Antibodies used in this study are listed in Table S4.

### RNA interference and plasmid transfections

C2C12 cells were plated at 60,000/ml and transfected with DharmaFECT (Thermo Fisher Scientific) according to the manufacturer's instructions. A mix of two siRNAs was used for each gene at a final concentration of 10 nM. 24 h after transfection, cells were diluted to 60,000/ml and transfected again under the same conditions. At confluence, cells were transfected again. 24 h after the final transfection, cells were collected as confluent MBs or induced to differentiate and collected at the indicated time points as MTs. The following sequences were purchased from Invitrogen: siRNA mEzh2 no. 1 (s65775; sense: 5'-GGAAAUUCCUGCUGAUAATT-3', antisense: 5'-UUAUCAGCAGGAAAUUCCGA-3'), siRNA mEzh2 no. 2 (s65776; sense: 5'-GAGUCCUCAUUGGUACUUAATT-3', antisense: 5'-UAAGUACC AAUGAGGACUACTA-3'), siRNA mLamA/C no. 1 (s69252; sense: 5'-GGCUUGUGGAGAUCGAUAATT-3', antisense: 5'-UUAUCGAU CUCCACAAGCCGC-3'), siRNA mLamA/C no. 2 (s69254; sense: 5'-CCAUGGUUGAGGACAAUGATT-3', antisense: 5'-UCAUUGUC CUCAACCAUGGTC-3'), siRNA mLamB1 no. 1 (s69256; sense: 5'-GGAAGUUUAUUCGCUUGAATT-3', antisense: 5'-UUCAAGCG

AAUAAACUCCCCA-3'), siRNA mLamB1 no. 2 (s69257; sense: 5'-CAUCAGUCAGUUACAAAUATT-3', antisense: 5'-UAUUUGUA ACUGACUGAUGTG-3'), siRNA Bmi1 no. 1 (s63006; sense: 5'-CGC UAAUGGACAUUGCCUATT-3', antisense: 5'-UAGGCAAUGUCCA UUAGCGTG-3'), and siRNA Bmi1 no. 2 (s63005; sense: 5'-GAG CAGAUUGGAUCGGAAATT-3', antisense: 5'-UUUCCGAUCCAAU CUGCUCTG-3'), as well as negative control siRNA (Stealth RNAi, 12935112, not targeting mouse or human genome).

Transient transfections with empty plasmids or plasmids containing wild-type human lamin A, obtained from H.J. Worman (Columbia University, New York, NY), were performed with Lipofectamine 2000 (Invitrogen) according to the manufacturer's instructions. Plasmid was cotransfected at a final concentration of 1.25  $\mu$ g/ml together with siRNA at a final concentration of 10 nM. The next day, a second round of siRNA transfection was performed with DharmaFECT. 24 h after the final transfection, cells were collected as confluent MBs. Myc-tagged human Ezh2, cloned into the pBABE retroviral vector (Addgene), or control empty vector was obtained from G. Caretti (University of Milan, Milan, Italy). Phoenix-Eco cells were obtained from ATCC and cultured in DMEM supplemented with 10% FBS (growth medium). Transient transfection of Phoenix-Eco cells was performed using lipofectamine reagent (Invitrogen), and viral particles were collected after 48 h. Supernatants containing viral particles were used to infect C2C12 cells. Medium was replaced after 24 h, and cells were transfected with siRNA against control or lamin A/C with DharmaFECT. After 24 h, siRNA transfection was repeated. After 24 h, cells were collected as confluent MBs.

**Satellite cells.** Muscle satellite cells were isolated from wild-type C57BL/6J adult (2-mo-old) mice, homozygous Lamin  $\Delta 8-11$  mice (LamA/C mut), and their wild-type littermates. Single muscle fibers were plated on matrigel-coated dishes and satellite cells were transfected with DharmaFECT according to the manufacturer's instructions. 48 h after transfection, cells were transfected again. 24 h after the final transfection, cells were collected.

**Human MBs.** Cells were plated at 60,000/ml and transfected with DharmaFECT according to the manufacturer's instructions. A mix of two siRNAs was used at a final concentration of 10 nM. At confluence, cells were transfected again. 24 h after the final transfection, cells were collected as confluent MBs or induced to differentiate and collected at the indicated time points as MTs. The following sequences were purchased from Invitrogen: siRNA hLamA/C no. 1 (s8221; sense: 5'-CCAAAAAGCGCAAACUGGATT-3', antisense: 5'-UCCAGUUU GCGCUUUUUGGTG-3') and siRNA hLamA/C no. 2 (s8222; sense: 5'-GAAGGAGGGUGACCUGAUATT-3', antisense: 5'-UAUCAGGU CACCCUCCUUCTT-3'), as well as negative control siRNA (Stealth RNAi, 12935112, not targeting mouse or human genome).

**Drosophila S2 cells.** Exonic fragments of 600, 1400, 810, or 356 bp from *Gfp*, *Pc*, *E(z)*, or *Lamin C* genes, respectively, were amplified by PCR, creating T7 polymerase binding sites for the transcription of both strands. RNAi was performed as described previously (Breiling et al., 2001). In brief, cells were diluted at 10<sup>6</sup>/ml and transfected with Fugene 6 (Promega) and 2  $\mu$ g dsRNA. Three rounds of transfection were performed. Primer sequences were as follows: *Gfp* 5'-ACGTAAAC GGCCACAAGTTC-3', 5'-TGCTCAGGTAGTGGTTGTGTCG-3'; *Pc* 5'-ATTGGCAAGTTAAGCACGGGCA-3', 5'-ACATCCTGGATCG CCGCTCA-3'; *E(z)* 5'-TCGAAGGCATTATGAATAGCAC-3', 5'-ATCCGCATCTTCAGTCTCC-3'; and *Lamin C* 5'-TTCGAGGA TCAGGCCAAGG-3', 5'-GCCTTGAGGTTCTGGATCTC-3'.

### Real-time PCR analysis

Total RNA was extracted from cells using TriReagent (Sigma-Aldrich) according to the manufacturer's instructions. 1  $\mu$ g RNA from each sample was subjected to cDNA synthesis using a QuantiTect reverse

transcription kit (Qiagen) and amplified in 20- $\mu$ l reaction mixtures in the presence of 10  $\mu$ l 2 $\times$  QuantiTect SYBR Green master mix (Qiagen) and 0.5  $\mu$ M corresponding primers. Real-time PCR was performed using DNA Engine Opticon 2 (MJ Research) or 7900HT (Applied Biosystems). Copy number was determined using the cross-point value, which is automatically calculated by Opticon Monitor 2 software (MJ Research) or SDS v2.3 software (7900HT). Mouse primer sequences used for transcriptional analyses were as follows: mRTGadph 5'-GTATGTCG TGGAGTCTACTGG-3', 5'-TCGTGGTTCACACCCATCAC-3'; mRT-MyoG 5'-GTACATTGAGCGCCTACAGG-3', 5'-ACCGAACTCCAGT GCATTGC-3'; mRTMCK 5'-GCTTCACTCTGGACGATGTC-3', 5'-CCTTGAAGACCGTGTAGGAC-3'; mRTMyHC 5'-TCAGGAAC CTTCGGAACACC-3', 5'-TCGATCTCAGCCTGCATCAG-3'; mRT-Mybph 5'-AGCCAGCATTGACATCCTG-3', 5'-TTGTCTGCCTTCT GTACTGTG-3'; mRTLamA/C 5'-CAATGGTGCCTGAGAGGC AG-3', 5'-GGCTTGACCTTCTCAGTCATC-3'; mRTEzh2 5'-TGA TAAAGAACTTGCCACCT-3', 5'-CTTTGCTCCCTCTGAACA GAT-3'; mRTDesmin 5'-GTATTGACCTGGAGCGCAG-3', 5'-CTG TGAGGTCCGGCTTGGA-3'; mRTNeuroG 5'-ACCTGTCCAGCTT CCTCAC-3', 5'-CACCGGGAACATTCGATGC-3'; mRTHoxD9 5'-TGAAGGAGGAGGAGAAGCAG-3', 5'-TCCTTCTCCAGCTCTAGC GT-3'; mRTLamb1 5'-AGTGGATTTGGAGAATCGCTG-3', 5'-GTA CTCATCACTCACTGACGC-3'; and mRTPax7 5'-GCTCTCAA GATTCTGTGCCGA-3', 5'-GGTCCCGGATTTCCACGC-3'. Human primer sequences used for transcriptional analyses were as follows: hRTGadph 5'-TCTGGTAAAGTGGATATTGTTGCC-3', 5'-CAA GCTTCCCGTTCTCAGCC-3'; hRTMyoG 5'-TCAACCAGGAGGA GCGTGAC-3', 5'-TGTAGGGTCAGCCGTGAGCA-3'; hRTMCK 5'-GACAGGAGTGGACAACCCAG-3', 5'-CGAGATGATGGGGTCAAA GAGTT-3'; hRTMyH2 5'-GGACCAACTGAGTGAAGTGA-3', 5'-TTGCCTCTTGATAACTGAGACAC-3'; hRTLamA/C 5'-GCTCTCAT CAACTCCACTGG-3', 5'-GGTCATCTCCATCCTCATCC-3'; and hRTPax7 5'-GCACTGTGCCCTCAGGTT-3', 5'-CCTCCTTCTTGTG CCGTTC-3'. *Drosophila* primer sequences used for transcriptional analyses were as follows: dRTGadph 5'-AAGGGAATCCTGGGCTAC AC-3', 5'-ACCGAACTCGTTGTCGTACC-3'; dRTPc 5'-TTCAAGAC TCAAGTGCTGCC-3', 5'-CCATGGGAAATAAGCAGGAG-3'; dRTEz 5'-CTGTGGCTGAGATCAACTCC-3', 5'-GACAGGTCTTGGT CAGCATG-3'; dRTUbx 5'-AGTGTGTCAGCGCGGCAAC-3', 5'-AGT CTGGTAGAAGTGAGCCCG-3'; dRTabdA 5'-CAAATACAACGCA ACCCGAGAC-3', 5'-AGCGATCGTGTGCTGCTG-3'; dRTLamC 5'-AACTCGATCGATCGGTGC-3', 5'-TACTGGGCGTGCCACTGC-3'; dRTLamDm0 5'-TGGGAGGAGAACGAGGAGC-3', 5'-ATC GGCGTTGGCCTGGTTG-3'; and dRTbw 5'-TCGCTGTGCCCTCG AGTGG-3', 5'-AATCGCCGCCAGCAGCG-3'.

### RNA sequencing

For high-throughput sequencing, cDNA libraries were prepared from total RNA and extracted with Trizol, according to the manufacturer's instructions (Illumina). cDNA fragments of ~300 bp were purified from each library and were sequenced for 100 bp with an Illumina HiSeq2500 instrument according to the manufacturer's instructions. The analysis was performed using fastqc to check the sequences' quality (Andrews, 2015); trim\_galore for quality-based trimming; tophat2 for alignment; and cufflinks, cuffmerge, and cuffdiff for expression quantification (Trapnell et al., 2012). Deregulated genes were determined to a P value lower than the false discovery rate after Benjamini-Hochberg correction for multiple testing. We used fold changes to filter and select differentially expressed genes with vennt (fold change R1.2). The hypergeometric distribution was computed using R software. GO analysis was performed with DAVID Bioinformatics Resources (Huang et al., 2009).

### Chromatin fractionation

High-salt chromatin fractionation was performed essentially as described (He et al., 1990), with minor adaptation. 35 million S2 cells or 8 million C2C12 cells were washed in PBS 1 $\times$  and extracted in cytoskeleton (CSK) buffer (10 mM Pipes, pH 6.8, 100 mM NaCl, 1 mM EGTA, 300 mM sucrose, 3 mM MgCl<sub>2</sub>, 1 $\times$  protease inhibitors [Roche Diagnostics], and 1 mM PMSF) supplemented with 1 mM DTT and 0.5% Triton X-100. After 5 min at 4°C, the cytoskeletal frameworks were separated from soluble proteins by centrifugation at 3,000 rpm for 3 min, and the supernatant was designated the S1 fraction. The pellets were washed with an additional volume of extraction CSK buffer. Chromatin was solubilized by DNA digestion with 25 U RNase-free DNase (Invitrogen) in CSK buffer for 30 min at 37°C. Ammonium sulfate was added in CSK buffer to a final concentration of 250 mM. After 5 min at 4°C, samples were pelleted again at 5,000 rpm for 3 min at 4°C, and the supernatant was designated the S2 fraction. After a wash in CSK buffer, the pellet was further extracted with 2M NaCl in CSK buffer for 5 min at 4°C and centrifuged at 5,000 rpm for 3 min at 4°C; the supernatant was designated the S3 fraction. This treatment removed all the DNA and histones from the nucleus, as shown by SDS-PAGE. After two washes in NaCl 2M CSK, the pellets were solubilized in 8M urea buffer and were considered the nuclear matrix-containing fraction (S4). Supernatants from each extraction step were quantified and analyzed by SDS-PAGE and immunoblotting. For DNA analysis, each fraction was diluted in Tris-EDTA 1 $\times$  (10 mM Tris-HCl, pH 8, and 1 mM EDTA), treated with 10 mg/ml RNase for 90 min at 37°C, digested with 20 mg/ml proteinase K for 150 min at 55°C, extracted by standard phenol/chloroform extraction, precipitated, and resuspended in 100  $\mu$ l of water. DNA was quantified with a Qubit Fluorometer (Life Technologies), and qPCR reactions were performed in triplicate on equal amounts of DNA from distinct fractions using QuantiTect SYBR Green master mix on a Rotor gene 6000. Cycle threshold (Ct) values were calculated by appropriate software. Fraction-specific relative enrichment was calculated as a percentage with respect to S1 + S2 + S3.

### Protein extraction and Western blot analyses

Total proteins were prepared by resuspending 2  $\times$  10<sup>6</sup> S2 cells or 500,000 C2C12 cells in extraction buffer (50 mM Tris HCl, pH 7.6, 0.15 M NaCl, 5 mM EDTA, 1 $\times$  protease Inhibitors, and 1% Triton X-100). Three pulses of 10-s sonication at 30% amplitude were performed to allow dissociation of protein from chromatin and solubilization. Extracts were analyzed by SDS-PAGE using a 12% gel for histones and an 8–10% gel (37.5:1 acryl/bis acrylamide) for the remaining proteins.

### coIP

coIP on nuclear extracts was performed using standard procedures. In brief, nuclear extracts were prepared after cytosolic extraction with cytosolic lysis buffer (10 mM Hepes, pH 7.5, 1.5 mM MgCl<sub>2</sub>, 10 mM KCl, 10% glycerol, 0.2% NP-40, 1 mM DTT, and protease inhibitors) for 10 min on ice and a 3/8-in syringe with a 25G needle. Nuclei pellets were then lysed in nuclei lysis buffer (10 mM Hepes, pH 7.5, 1.5 mM MgCl<sub>2</sub>, 300 mM KCl, 10% glycerol, 0.2% NP-40, 1 mM DTT, and protease inhibitors) for 30 min at 4°C. 0.5 to 1 mg of nuclear extract was immunoprecipitated overnight at 4°C with 5  $\mu$ g corresponding antibodies at a final concentration of 150 mM KCl in nuclei lysis buffer. Immunoprecipitates were incubated with magnetic protein G beads (10004D; Dynabeads; Invitrogen) for 2 h at 4°C. Beads were extensively washed with wash buffer (10 mM Hepes, pH 7.5, 1.5 mM MgCl<sub>2</sub>, 150 mM KCl, 0.2% NP-40, and 10% glycerol) and eluted in Tris-EDTA 1 $\times$ . Finally, beads were resuspended in Laemmli buffer and boiled at 95°C for 5 min, and the supernatant was analyzed by Western blot.

**Chromatin immunoprecipitation (ChIP)**

**C2C12 cells.** MBs or MTs at 4 d after differentiation induction (MT4) were cross-linked with HCHO 1% for 12 min, lysated, and chromatin-sheared using a Branson Digital Sonifier 250. Chromatin IP was performed overnight on the wheel at 4° with 5 µg Ezh2 antibody or 7 µg lamin A/C antibody. The next day, antibodies and chromatin immunocomplexes were loaded onto protein G beads. For Ezh2 IP, the bound complexes were washed twice in low-salt solution (0.1% SDS, 2 mM EDTA, 1% Triton X-100, 20 mM Tris, pH 8, and 150 mM NaCl), twice in high-salt solution (0.1% SDS, 2 mM EDTA, 1% Triton X-100, 20 mM Tris, pH 8, and 500 mM NaCl), once in LiCl (250 mM LiCl, 1% NP-40, 1 mM EDTA, and 10 mM Tris, pH 8), and twice in Tris-EDTA and 50 mM NaCl. For lamin A/C IP, the bound complexes were washed once in low-salt solution, once in high-salt solution, once in low-salt solution, and once in Tris-EDTA and 50 mM NaCl. Cross-linking was reversed at 65°C overnight in elution buffer (50 mM Tris, pH 8, 10 mM EDTA, and 1% SDS), and DNA was extracted from beads by standard phenol/chloroform extraction, precipitated, and resuspended in 20 µl of 10-mM Tris, pH 7.5. qPCR reactions were performed in triplicate or duplicate (precipitated DNA samples as well as serially diluted input DNA) using QuantiTect SYBR Green master mix or Power SYBR Green PCR master mix (Life Technologies) on a DNA Engine Opticon 2 or Step One Plus (Applied Biosystems). Ct values were calculated by appropriate software. Relative enrichment was calculated as ChIP/input ratio. Primer sequences were as follows: MCK enh 5'-GAC ACCCGAGATGCCTGGTT-3', 5'-GATCCACCAGGGACAGGG TT-3'; MCK 5'-TACTGTTCCATGTTCCCGCGAAG-3', 5'-TAG AGGAGCCTACAGGGTGTGACTAG-3'; MyoG 5'-TGGCTATA TTTATCTCTGGGTTCA-3', 5'-GCTCCCGCAGCCCCT-3'; Mybph 5'-AGCATGAACCTAGCCTGGAG-3', 5'-AAGGCTCTGTAGT GGGCACC-3'; Desmin 5'-GCTACAAATAGTGCAGACAGC-3', 5'-TGGACGAGTAGGCCTGGCT-3'; NeuroG1 5'-AGAGACAC CGCTACTAGGCA-3', 5'-GCACTGGACTGGAGGGTAC-3'; HoxD9 5'-AGAGTCCGGGTGGAGATCG-3', 5'-CATCATCAACAGG AGCGTTGC-3'; Pax7-PRE 5'-TGAACTGGAGCCCTGAGAA-3', 5'-CAGGGTACCCCTCCCAAGT-3'; ACPP 5'-TTGCATGC TAAGCTCTGCCC-3', 5'-GAACGGCTCGCATGGTCG-3'; OLF681 5'-CTTCATATATTCAGAGTCAGAAC-3', 5'-GTTGGTGTGTTT TGTGTGC-3'; SP100 5'-GCTTGGGCTCACTTCTGC-3', 5'-TCG CTCCCTCCATCTTCC-3'; and Sun1p0 5'-CTTCAGCAGGCGC GCTTGG-3', 5'-TCAGGCCTCGTCCGACC-3'.

**Drosophila.** Cells were fixed in 1% formaldehyde for 15 min at RT and quenched by addition of glycine at 125 mM final concentration for 5 min at RT before being placed on ice. Cells were washed once with ice-cold PBS, resuspended in ice-cold cell lysis buffer (5 mM Pipes, pH 8, 85 mM KCl, 0.5% NP-40, 1 mM PMSF, and 1× protease inhibitors) and left on ice for 10 min. After centrifugation at 2,000 rpm for 5 min, nuclei were resuspended in ice-cold nuclear lysis buffer (50 mM Tris HCl, pH 8.0, 10 mM EDTA, 0.8% SDS, 1 mM PMSF, and 1× protease inhibitors) and left for 10 min on ice. Chromatin was sonicated in the presence of glass beads (150–200 µm; Sigma-Aldrich), spun for 10 min at maximum speed at 4°C, diluted to 0.2% SDS with dilution buffer (10 mM Tris HCl, pH 8.0, 0.5 mM EGTA, 1% Triton X-100, and 140 mM NaCl), then split into aliquots and processed immediately for IP. For preclearing and antibody recovery, Protein A/G Plus agarose beads (Santa Cruz Biotechnology) were used. After washing, samples and control chromatin (input) were incubated in the presence of 2 ml RNase cocktail (DNase-free; Ambion) overnight at 65°C. Samples were adjusted to 0.5% SDS and 0.5 mg/ml proteinase K and incubated for an additional 2 h at 55°C. DNA was phenol–chloroform extracted and precipitated. The final pellet was resuspended in 30 µl Tris-EDTA and stored at 4°C for RT-PCR analysis. Primer sequences were as follows:

mcp-1 5'-TCACTTGAGCCGCATTCC-3', 5'-TAGGTGTTGCCAC CGCAC-3'; mcp 5'-TGCGGACGCCATTTGACAC-3', 5'-GAG CCACGACGAGTTC-3'; mcp+1 5'-TACAGCATTTTCAGGTGCC ACG-3', 5'-CACCATTGTGTCGTCATAAAGCGTC-3'; bxd-1 5'-AGA TTCTGAAATGTCGCCTTGC-3', 5'-AGTGCTGCGGGACCATCC-3'; bxd 5'-GTAATTATCCAAACAAGCGACGG-3', 5'-AGTTATCG GCACCTTTGGTTC-3'; bxd+1 5'-TTGAATAATGCCGGCATCGG-3', 5'-GAATGCATGTGGCCGATGG-3'; Ubxp-1 5'-TTAATCTA CGAGCCGTTTGTGC-3', 5'-CAAATGTTCAATCCGTTCCGC-3'; Ubxp 5'-TCAGCCCTCCTCCATGATG-3', 5'-CCAAATCGCAGTT GCCAGTG-3'; Ubxp+1 5'-CTTTCCTACTAGATTGGCGTCC-3', 5'-TTGGATTGCGCTTGCCTTGG-3'; abdA-1 5'-GAGAGCAATAGTA GAAGAGGC-3', 5'-AGTGCGCTGCCTTTGAGTG-3'; abdAp 5'-TTGAGTCAGGGAGTGAGCC-3', 5'-CGCTTTGAGTCGTTGGAG AC-3'; abdA+1 5'-CAAATACAACGCAACCCGAGA-3', 5'-TGC CAGTGCCAACGAGTTAG-3'; and bwp 5'-TGATGAGCGACAA TTAGCTGG-3', 5'-TGTCCGTCTGTCTGTCTGTC-3'.

**Microscope image acquisition**

For immunofluorescence assay of *Drosophila* S2 cells, coverslips were fixed in 4% paraformaldehyde and 1× PBS for 10 min at RT. Cells were washed three times with PBT (PBS 1× and 0.1% Tween 20) and incubated for 1 h at RT with RNaseA (100 mg/ml in PBT) and for 10 min at RT with PBS and 0.5% Triton X-100. After being washed again in PBS, the cells were blocked in PBS/1% BSA. All antibody hybridizations were performed in a humid atmosphere at 37°C. Anti-PC antibodies were diluted 1:200 and incubated for 12–16 h at 4°C. After three washes in PBT, cells were stained with appropriate secondary antibodies, diluted 1:1,000 for 1 h at 37°C, and washed in PBT. DNA was counterstained with DAPI, and glasses were mounted in Vectashield Antifade (Vector Laboratories) or ProLong Gold Antifade Reagent (Invitrogen).

For C2C12 cells, satellite cells, and human MBs, coverslips were fixed with 4% paraformaldehyde in PBS for 10 min. Cells were permeabilized with 0.5% Triton X-100 in PBS, and aspecific signals were blocked with 1% BSA in PBS for 30 min at RT. Reaction with primary antibodies Ezh2 and Bmi1, diluted 1:100, was performed for 12–16 h at 4°C; incubation with MyH diluted 1:200, lamin B diluted 1:200, or lamin A/C diluted 1:200 was performed at RT for 2 h. Primary antibodies were diluted in a PBS solution containing 1% BSA. Cells were stained with appropriate secondary antibodies, diluted 1:200, for 1 h at RT and washed in PBT. DNA was counterstained with DAPI, and glasses were mounted in Vectashield Antifade or ProLong Gold Antifade Reagent. For BrdU labeling, cells were grown in the presence of 50 µM BrdU for 4 h (C2C12 cells), 8 h (satellite cells), or 48 h (human MBs). After treatment with Triton X-100, cells were incubated for 2 min at RT in 0.07N NaOH, briefly rinsed twice in PBS, and blocked in PBS/1% BSA. Reaction with BrdU antibodies, diluted 1:10, was performed at RT for 1 h in a PBS solution containing BSA 1%.

For PLA experiments, coverslips were fixed with 4% paraformaldehyde in PBS for 10 min. Cells were permeabilized with 0.5% Triton X-100 in PBS and blocked with 1% BSA in PBS for 1 h at RT. Detection of protein interactions was performed using the Duolink system (Sigma-Aldrich) according to the manufacturer's instructions.

**Secondary antibodies.** Alexa Fluor 594 donkey anti-mouse IgG (715-585-150), Alexa Fluor 488 donkey anti-rabbit IgG (711-545-152), Alexa Fluor 594 donkey anti-rabbit IgG (711-585-152), Alexa Fluor 488 donkey anti-mouse IgG (715-545-150), Alexa Fluor 594 donkey anti-goat IgG (705-585-003), and Alexa Fluor 488 donkey anti-goat IgG (705-545-003) were from Jackson ImmunoResearch Laboratories.

**Immunoelectron microscopy.** Cells were fixed with 4% paraformaldehyde in 0.1 M cacodylate buffer for 1 h, and then in 1% glutaraldehyde and 0.1 M cacodylate buffer for 1 h at 4°C. Samples

were dehydrated in an ethanol series and embedded in EPON resin. Thin sections were collected on nickel grids, preincubated with 5% normal goat serum, incubated with anti-Bmi-1 antibody (05-637; Millipore) diluted 1:10 in TBS overnight at 4°C, and incubated with goat anti-mouse antibody conjugated with 10 nm colloidal gold, diluted 1:10 in TBS, for 1 h at RT; some grids underwent colloidal gold amplification with a Silver Enhancer kit. The controls consisted of samples not incubated with the primary antibody. Grids containing ultrathin sections were stained with uranyl-acetate and lead citrate and observed with a Jeol Jem-1011 transmission electron microscope at 100 kV. The experiment was repeated twice with similar results.

**3D-SIM acquisition and quantification.** Fixed samples were prepared by treatment with 4% platelet-activating factor for 10 min at RT, followed by permeabilization (10 min in PBS and 0.5% Triton X-100) and primary antibody staining for 2 h at RT in PBS and 1% BSA. After several washes in PBT, samples were hybridized with the Alexa Fluor 488- and 568-conjugated secondary antibodies for 1 h at RT. Superresolution imaging on prepared samples was performed with an N-SIM microscope system (Nikon) equipped with a CFI Apo TIRF 100× 1.49 N.A. oil immersion objective and a 897EMCCD Andor camera. 3D-SIM image stacks were acquired with a  $z$ -distance of 0.24  $\mu\text{m}$ , covering a range of 5.76  $\mu\text{m}$  (25 stacks/nucleus) using laser power setting 25% and 100-ms exposition time. With this setting, 15 raw images per plane were acquired and computationally reconstructed using the reconstruction slice system from NIS-Elements AR software (version 4.20.01; Nikon). Minimal distance measurements were performed using Volocity (Perkin Elmer) with the find spot function, which allowed us to identify the brightest spots within a 0.05- $\mu\text{m}$  radius in each channel. After the measurement of minimal distance, the results were analyzed by plotting their distribution.

### Image analysis

Fluorescent images were taken of fixed samples at RT with a Nikon Eclipse 90i microscope (100× objective) that was equipped with a digital camera (Nikon Coolpix 990) and NIS Element software or with a confocal Leica SP5 (63× objective) supported by LAS-AF software. Fluorochromes are indicated in the figure legends. Magnification of the objective is 63×. Fluorescence quantification was done by determining the intranuclear mean fluorescence intensity using Cell Profiler 2.0 (Carpenter et al., 2006) that computes area, form factor (Russ, 2011), integrated intensity, and mean intensity. PLA blob quantification was performed using Cell Profiler 2.0. Nuclei were detected using the Otsu method with a global two-class threshold strategy, and foci were detected using the Otsu method with a per-object three-class threshold strategy (Otsu, 1979). PcG foci quantification was performed with an automated pipeline that executes the following steps: loads images with DAPI- or lamin B-stained nuclei and PcG protein immunofluorescence, converts images to grayscale, performs segmentation with the IdentifyPrimaryObject algorithm using a two-class Otsu global threshold method (Otsu, 1979), locates nuclei regions on DAPI or lamin B images, discards partial nuclei at the image borders, and measures PcG protein-stained image intensity, size, and shape of nuclei. Confocal image size is 1,024 × 1,024 pixels, and the number of stack planes on the  $z$ -axis varies between 24 and 36.

The software proposed for the segmentation of fluorescence images, written in C, relies on two novel algorithms and works on two image stacks that include the staining for lamin B or DAPI and Bmi1, Ezh2, or PC. The first algorithm, modified Chan-Vese (MCV), provides image contours as curves that match the object's edges, producing a two-phase partition of images: nuclei regions and background. We adopted a modified version of the local Chan-Vese Active Contour model proposed in Wang et al. (2010), described by the following functional:  $E^{MCV}(c_1, c_2, d_1, d_2, C) = \mu \text{Length}(C) + \alpha \left[ \int_{\text{inside}(C)} |I - c_1|^2 dx dy + \int_{\text{outside}(C)} |I - c_2|^2 dx dy \right] + \beta \left[ \int_{\text{inside}(C)} |I^* - I - d_1|^2 dx dy + \int_{\text{outside}(C)} |I^* - I - d_2|^2 dx dy \right]$ . The

functional controls the evolution of the curve  $C$  by means of three terms weighted by positive parameters  $\mu$ ,  $\alpha$ , and  $\beta$ , respectively. The first term is the regularization term measuring the perimeter of  $C$  (internal forces). The second two terms represent the edge-detector (external forces) that attracts the curve toward the nuclei boundaries. The second term is the sum of the intensity variances of the regions of  $I$  inside and outside  $C$ , respectively, where  $I$  is the lamin B or DAPI image and  $c_1$  and  $c_2$  are the mean intensity values of regions of  $I$  inside and outside  $C$ , respectively. The third term, different from the one used in Wang et al. (2010), enforces the contrast between the nuclei regions and image background by incorporating statistical information on both lamin B or DAPI and Bmi1, Ezh2, or PC images. In fact,  $I^*$ , from which we subtract the original lamin B or DAPI image, is obtained as the sum of  $g_k(I)$  and  $g_k(I^C)$ , where  $g_k$  is the averaging convolution operator with  $k \times k$  window, and  $I^C$  is the Bmi1, Ezh2, or PC fluorescence image. This term represents the sum of the intensity variances of the regions of the composite image  $I^* - I$  inside and outside  $C$ , respectively, where  $d_1$  and  $d_2$  are the mean intensity values of  $I^* - I$  inside and outside  $C$ , respectively. The edge-detector acts by adaptively balancing the intensity variances of the nuclei regions and image background. The evolution of  $C$  stops when an optimal partition of the image into two regions is achieved. Mathematically, this is equivalent to finding the minimum of the functional  $E^{MCV}(c_1, c_2, d_1, d_2, C)$ . The minimization problem is usually solved by means of level set methods, where the curve  $C$  is represented by the zero level set of a Lipschitz function defined on the image domain  $\Omega$ , with values in the set of real numbers such that  $C = \{(x, y) \in \Omega \text{ such that } \phi(x, y) = 0\}$ ;  $\text{inside}(C) = \{(x, y) \in \Omega \text{ such that } \phi(x, y) < 0\}$ ; and  $\text{outside}(C) = \{(x, y) \in \Omega \text{ such that } \phi(x, y) > 0\}$ .

The expression of the functional  $E^{MCV}$  in terms of function  $\phi$  is analogous to the one of the functional  $E^{LCV}$  described in Wang et al. (2010), where  $\text{Length}(C) = \int_{\Omega} \delta_{\epsilon} \phi(x, y) |\nabla \phi(x, y)| dx dy$ , and  $\delta_{\epsilon}$  is a smoothed version of the one-dimensional Dirac function. The functional  $E^{MCV}$  is minimized by computing the Euler-Lagrange equation and then solving the resulting partial differential equation (PDE) by the gradient flux method. Unlike in Wang et al. (2010) where an explicit scheme is used, we used a time-dependent semi-implicit scheme to discretize Euler-Lagrange equations. Although the use of an implicit time discretization scheme requires greater computational effort than an explicit one, it is compensated for by the unconditional stability of the numerical algorithm. Furthermore, usually segmentation of high-dimensional images (such as fluorescence images) requires many iterations to converge to a numerical solution. By adopting an implicit scheme, we can reduce the number of iterations, allowing the choice of larger time steps. To recall the usual notations for the finite difference methods: let  $h$  be the space step,  $dt$  be the time step, and  $(x_i, y_j) = (ih, jdt)$  be the grid points for  $1 \leq i, j \leq M$ . Let  $\phi_{ij}^n = \phi(ndt, x_i, y_j)$  be an approximation of  $\phi(t, x, y)$  with  $n \geq 0$ ,  $\phi^0 = \phi_0$ , and we have the following time-dependent PDE:

$$\frac{\phi_{ij}^{n+1} - \phi_{ij}^n}{dt} = \delta_{\epsilon}(\phi_{ij}^n) \left\{ \frac{\mu}{h^2} \left[ \frac{\phi_{i+1,j}^n - \phi_{ij}^{n+1}}{\sqrt{\epsilon^2 + \left(\frac{\Delta_x^2 \phi_{ij}^n}{h}\right)^2 + \left(\frac{\Delta_y^2 \phi_{ij}^n}{2h}\right)^2}} + \frac{\phi_{ij}^{n+1} - \phi_{i-1,j}^n}{\sqrt{\epsilon^2 + \left(\frac{\Delta_x^2 \phi_{ij}^n}{h}\right)^2 + \left(\frac{\Delta_y^2 \phi_{i-1,j}^n}{2h}\right)^2}} + \frac{\phi_{ij}^{n+1} - \phi_{i,j+1}^n}{\sqrt{\epsilon^2 + \left(\frac{\Delta_x^2 \phi_{ij}^n}{h}\right)^2 + \left(\frac{\Delta_y^2 \phi_{ij}^n}{2h}\right)^2}} + \frac{\phi_{ij}^{n+1} - \phi_{i,j-1}^n}{\sqrt{\epsilon^2 + \left(\frac{\Delta_x^2 \phi_{ij}^n}{h}\right)^2 + \left(\frac{\Delta_y^2 \phi_{i,j-1}^n}{2h}\right)^2}} \right] - \lambda_1 [I_{ij} - c_1(\phi^n)]^2 + \lambda_2 [I_{ij} - c_2(\phi^n)]^2 \right\}$$

where  $\Delta_{\pm}^x \phi_{ij} = \pm(\phi_{i\pm 1j} - \phi_{ij})$ ,  $\Delta_{\pm}^y \phi_{ij} = \pm(\phi_{ij\pm 1} - \phi_{ij})$ ,  $\Delta_{\delta}^x \phi_{ij} = \pm(\phi_{i+1j} - \phi_{i-1j})$ , and  $\Delta_{\delta}^y \phi_{ij} = \pm(\phi_{ij+1} - \phi_{ij-1})$ .

Finally, we solved the time-dependent PDE with respect to  $\phi_{ij}^{n+1}$  as follows:

$$\phi_{ij}^{n+1} = \left\{ \frac{h}{h + dt[\delta_x(\phi_{ij}^n)\mu - 1](C_1 + C_2 + C_3 + C_4)} \right\} \cdot \left( \begin{aligned} & \phi_{ij}^n + dt \delta_x(\phi_{ij}^n) \mu (C_1 \phi_{i+1j}^{n+1} + C_2 \phi_{i-1j}^{n+1} + C_3 \phi_{ij+1}^{n+1} + C_4 \phi_{ij-1}^{n+1}) \\ & - dt \delta_x(\phi_{ij}^n) \left\{ \lambda_1 [I_{ij} - c_1(\phi^n)]^2 - \lambda_2 [I_{ij} - c_2(\phi^n)]^2 \right\} \end{aligned} \right), \quad (1)$$

where

$$C_1 = \frac{1}{\sqrt{\epsilon^2 + \left(\frac{\Delta_x^2 \phi_{ij}^n}{h}\right)^2 + \left(\frac{\Delta_y^2 \phi_{ij}^n}{2h}\right)^2}} + \frac{1}{h[\mu \delta_x(\phi_{ij}^n) - 1]};$$

$$C_2 = \frac{1}{\sqrt{\epsilon^2 + \left(\frac{\Delta_x^2 \phi_{ij}^n}{h}\right)^2 + \left(\frac{\Delta_y^2 \phi_{ij}^n}{2h}\right)^2}} + \frac{1}{h[\mu \delta_x(\phi_{ij}^n) - 1]};$$

$$C_3 = \frac{1}{\sqrt{\epsilon^2 + \left(\frac{\Delta_x^2 \phi_{ij}^n}{h}\right)^2 + \left(\frac{\Delta_y^2 \phi_{ij}^n}{2h}\right)^2}} + \frac{1}{h[\mu \delta_x(\phi_{ij}^n) - 1]};$$

$$C_4 = \frac{1}{\sqrt{\epsilon^2 + \left(\frac{\Delta_x^2 \phi_{ij}^n}{h}\right)^2 + \left(\frac{\Delta_y^2 \phi_{ij}^n}{2h}\right)^2}} + \frac{1}{h[\mu \delta_x(\phi_{ij}^n) - 1]}.$$

Principal MCV algorithm steps are MCV(in:  $I, I^G$ ; out:  $\phi^{k*}$ ) { $n = 0$  initialize  $\phi^0$  by  $\phi_0$ , compute  $I^k = g_k(I) + g_k(I^G)$ ,  $k = 1$ , for  $n = 1, 2, \dots, K$ , compute  $c_1[\phi^{n-1}(I)]$ ,  $c_2[\phi^{n-1}(I)]$ ,  $d_1[\phi^{n-1}(I^* - I)]$  and  $d_2[\phi^{n-1}(I^* - I)]$ , compute  $\phi^n$  from Eq. 1, if  $|\text{Length}(C^n) - \text{Length}(C^{n-1})| < T_L$  then, if  $k = T_i$  then, stop evolution curve, endif,  $k = k + 1$ , else,  $k = 1$ , endif, endfor} where the termination criterion is the one presented in (Wang et al., 2010) and  $K^* \leq K$  is the last iteration step.

Because PcG protein foci corresponded to image regions with highest intensity values, we used a thresholding approach to separate them from nucleus regions. The second algorithm, modified isodata (MID), modifies the ISODATA method (Ball and Hall, 1965) by using relevant values computed by the MCV algorithm to extract PcG foci from the nuclei regions. ISODATA is an unsupervised classification algorithm that splits and merges nonhomogeneous image regions into two subregions, based on a threshold. Usually ISODATA assigns the mean intensity value of the entire image as the initial value of the threshold, but it was misleading for our purpose of detecting PcG protein bodies that correspond to image regions within nucleus regions with highest intensity values; the mean intensity value of nucleus regions seemed like a more reliable choice for the initial threshold. Therefore, we set the initial threshold value as the mean intensity value of the nucleus regions, computed by the MCV algorithm. To enhance high-intensity areas, the MID algorithm initializes the first nonhomogeneous regions to be split as the nucleus regions of the images obtained by subtracting from the original *Bmi1*, *Ezh2*, or *PC* images the corresponding smoothed images. The MID algorithm can be summarized as follows: MID{in:  $c_1[\phi^{k*}(I^G)]$ ,  $I^G$ ; out:  $t$ } {initialize  $t = c_1[\phi^{k*}(I^G)]$ , compute  $\bar{I} = |I^G - g_k(I^G)|$ , repeat, split  $\bar{I}$  into  $R_1$  and  $R_2$  regions by means of  $t$ , compute  $m_1 = \text{mean of } R_1 \text{ intensity values}$ , compute  $m_2 = \text{mean of } R_2 \text{ intensity values}$ ,  $t = \text{average}(m_1, m_2)$ , until the difference in  $t$  in successive iterations is smaller than a predefined tolerance}.

Given the image stacks  $I_j$  and  $I_j^G$  for  $1 \leq j \leq N$ , the combined MCV-MID algorithm steps are  $\phi_j = \text{MCV}(I_j, I_j^G)$ , detect nuclei regions

and background for the entire stack images by using  $\phi_j$ , compute  $c_1[\phi_j(I_j^G)]$ ,  $t_j = \text{MID}\{c_1[\phi_j(I_j^G)], I_j^G\}$ , for  $j = 1, 2, \dots, N$ , compute  $c_1[\phi_j(I_j^G)]$ ,  $t_j = \text{MID}\{c_1[\phi_j(I_j^G)], I_j^G\}$ , detect PcG foci for stack section  $j$  by using  $\max(t_j, t_j)$ , endfor, where  $j$  is the middle section of the stack if not defined by the user.

Segmented image stacks produced by the software are “trinary” images: regions are segmented as background, nuclei, and PcG foci. Images were segmented by applying a fixed threshold computed by averaging threshold values performed by the MCV-MID algorithm on control images. In this way, we used a detection method that is homogeneous within populations, ensuring consistent results within the same biological replicate. The segmented stack is then used as input of the 3D Object Counter ImageJ plugin that performs the 3D reconstruction of the PcG foci, estimating their volume.

### 3C

The 3C assay was performed as previously described (Lanzuolo et al., 2007). In brief,  $10^7$  cells were cross-linked in 45 ml serum-free medium with 1% formaldehyde for 15 min at RT. The reaction was quenched by the addition of glycine to a final concentration of 0.125 M. Cells were centrifuged at 2,000 rpm, resuspended in 1 ml of 4°C cold cell lysis buffer (10 mM Tris, pH 8.0, 10 mM NaCl, 0.2% NP-40, and protease inhibitors), and incubated on ice for 1 h. Samples were kept on ice from this point onward. Cell lysis was completed with a syringe. Nuclei were washed with 0.5 ml restriction enzyme buffer, divided into aliquots (5 million/pellet), pelleted, and stored at  $-80^\circ\text{C}$ . Nuclei were thawed and resuspended in 362  $\mu\text{l}$  restriction enzyme buffer. SDS was added to a final concentration of 0.1%, and nuclei were incubated at  $37^\circ\text{C}$  for 15 min. Triton X-100 was added to a final concentration of 1% to sequester SDS. Digestion was performed with 400 U HindIII restriction enzyme at  $37^\circ\text{C}$  for 1.5 h. The restriction enzyme was inactivated by the addition of SDS to 2% and incubation at  $65^\circ\text{C}$  for 30 min. The reaction was diluted into 8 ml ligation reaction buffer (1% Triton X-100, 50 mM Tris, pH 7.5, 10 mM  $\text{MgCl}_2$ , 10 mM DTT, 0.1 mg ml $^{-1}$  BSA, 1 mM ATP, and 4000 U T4 DNA Ligase [New England Biolabs]). Ligation was performed at  $16^\circ\text{C}$  for 2 h. EDTA to a concentration of 10 mM was added to stop the reactions. Samples were treated with 500  $\mu\text{g}$  proteinase K and incubated for 5 h at  $50^\circ\text{C}$ , and then overnight at  $65^\circ\text{C}$  to reverse the formaldehyde cross-links. The next day, DNA was purified by phenol extraction and ethanol precipitation. Samples were redissolved in deionized water and quantified by RT-PCR. Primer sequences were as follows: int2-up 5'-TTATCCACGGACGGCAGTC-3'; int2-low 5'-TCTGTGGGATTTGTGGGATC-3'; AbdBp-up 5'-ATAGATGGCTGAGTGAGAG-3'; Fab7-up 5'-CTCACTTCTCCATGGCCTG-3'; mcp22b-up 5'-ATAGAAGTCAACATCCAGGC-3'; mcp23-up 5'-GGCCTGTGCAAGGAACGC-3'; abdAp-up 5'-ATGGCGCCAATGTCTCTG-3'; bxd-up 5'-CCTTAGCACGTTGTCAAGTG-3'; and bx-up 5'-AGTGATAATTGTCCGGGAG-3'.

### Online supplemental material

Fig. S1 shows two distinct cell phenotypes caused by *Lamin A/C* depletion. Fig. S2 shows the deregulation of PcG-regulated muscle genes after *Lamin A/C* depletion. Fig. S3 shows the muscle targets up-regulated after *Ezh2* and/or *Lamin A/C* depletion and the aberrant compartmentalization of PcG proteins and PcG protein targets after *Lamin A/C* depletion. Fig. S4 shows PcG protein-altered intranuclear localization after *Lamin A/C* depletion. Fig. S5 shows PcG protein aberrant localization and function after *Lamin C* depletion in *Drosophila*. Table S1 provides a list of antibodies used in this study. Table S2 provides a list of genes up-regulated in *Lamin A/C* KD. Table S3 provides a list of genes commonly up-regulated in *Ezh2* KD and *Lamin A/C* KD. Table S4 provides a list of genes up-regulated in

Lamin A/C KD and not in Ezh2 KD. Online supplemental material is available at <http://www.jcb.org/cgi/content/full/jcb.201504035/DC1>. Additional data are available in the JCB DataViewer at <http://dx.doi.org/10.1083/jcb.201504035.dv>.

## Acknowledgments

We are grateful to Davide Gabellini, Pier Lorenzo Puri, Giovanna Lattanzi, Gisele Bonne, Maria Vivo, and the Italian network of Laminopathies for stimulating discussions and constructive criticism. We thank Marco Cicuttin from Nikon Instruments S.p.a., Carlo Di Cristo, Valeria Berno, Alessandro Cherubini, Fulvio Florenzano, Jorge Cancino, and Alberto Luini for providing support for confocal microscopy in image acquisition. We thank Francesco della Valle, Andrea Bianchi, and Mariangela Panetta for help with cell cultures. We gratefully acknowledge Dr. Marina Mora for providing primary human myoblasts, H.J. Workman for plasmid containing human lamin A, and P. Fisher and R. Paro for providing antibodies that have been essential for this study.

This work was supported by grants from the Italian Ministry of Education, University, and Research (Futuro in Ricerca RBF106S1Z\_001) and the flagship Consiglio Nazionale delle Ricerche project (Epigen).

The authors declare no competing financial interests.

Author contributions: E. Cesarini and C. Lanzuolo designed the experiments and performed transfections, immunofluorescence, chromatin fractionations, ChIP, Western blots, and transcriptional analysis; C. Mozzetta and E. Cesarini performed colP; C. Mozzetta and A. Gargiulo performed experiments on murine satellite cells; F. Marullo and D. Palacios performed PLA experiments; A. Cortesi and B. Bodega performed lamin A/C ChIP; E. Cesarini, S. Di Pelino, and A. Zippo performed superresolution microscopy; M. Columbaro and S. Squarzone performed EM; F. Gregoretti, L. Antonelli, and G. Oliva performed image analysis; G. Oliva and C. Lanzuolo analyzed RNA sequencing data; E. Cesarini, C. Mozzetta, F. Marullo, F. Gregoretti, A. Cortesi, L. Antonelli, D. Palacios, A. Zippo, B. Bodega, and G. Oliva edited the manuscript; C. Lanzuolo conceived and supervised the study, interpreted the results, and wrote the paper; and all authors discussed and interpreted the results.

Submitted: 8 April 2015

Accepted: 28 September 2015

## References

Andrews, S. 2015. FastQC A Quality Control tool for High Throughput Sequence Data. Available at: <http://www.bioinformatics.babraham.ac.uk/projects/fastqc/> (accessed October 30, 2015).

Asp, P., R. Blum, V. Vethanatham, F. Parisi, M. Micsinai, J. Cheng, C. Bowman, Y. Kluger, and B.D. Dynlacht. 2011. Genome-wide remodeling of the epigenetic landscape during myogenic differentiation. *Proc. Natl. Acad. Sci. USA*. 108:E149–E158. <http://dx.doi.org/10.1073/pnas.1102223108>

Ball, G., and D. Hall. 1965. ISODATA: A novel method of data analysis and pattern classification. Stanford Research Institute, Menlo Park, CA. 72 pp.

Bantignies, F., and G. Cavalli. 2011. Polycomb group proteins: repression in 3D. *Trends Genet.* 27:454–464. <http://dx.doi.org/10.1016/j.tig.2011.06.008>

Bantignies, F., V. Roue, I. Comet, B. Leblanc, B. Schuettengruber, J. Bonnet, V. Tixier, A. Mas, and G. Cavalli. 2011. Polycomb-dependent regulatory contacts between distant Hox loci in *Drosophila*. *Cell*. 144:214–226. <http://dx.doi.org/10.1016/j.cell.2010.12.026>

Beard, G.S., J.M. Bridger, I.R. Kill, and D.R. Tree. 2008. Towards a *Drosophila* model of Hutchinson-Gilford progeria syndrome. *Biochem. Soc. Trans.* 36:1389–1392. <http://dx.doi.org/10.1042/BST0361389>

Bolte, S., and F.P. Cordelières. 2006. A guided tour into subcellular colocalization analysis in light microscopy. *J. Microsc.* 224:213–232. <http://dx.doi.org/10.1111/j.1365-2818.2006.01706.x>

Breiling, A., B.M. Turner, M.E. Bianchi, and V. Orlando. 2001. General transcription factors bind promoters repressed by Polycomb group proteins. *Nature*. 412:651–655. <http://dx.doi.org/10.1038/35088090>

Caretti, G., M. Di Padova, B. Micales, G.E. Lyons, and V. Sartorelli. 2004. The Polycomb Ezh2 methyltransferase regulates muscle gene expression and skeletal muscle differentiation. *Genes Dev.* 18:2627–2638. <http://dx.doi.org/10.1101/gad.1241904>

Carpenter, A.E., T.R. Jones, M.R. Lamprecht, C. Clarke, I.H. Kang, O. Friman, D.A. Guertin, J.H. Chang, R.A. Lindquist, J. Moffat, et al. 2006. CellProfiler: Image analysis software for identifying and quantifying cell phenotypes. *Genome Biol.* 7:R100. <http://dx.doi.org/10.1186/gb-2006-7-10-r100>

Cmarko, D., P.J. Verschuer, A.P. Otte, R. van Driel, and S. Fakan. 2003. Polycomb group gene silencing proteins are concentrated in the perichromatin compartment of the mammalian nucleus. *J. Cell Sci.* 116:335–343. <http://dx.doi.org/10.1242/jcs.00225>

Cohen, T.V., V.F. Gnocchi, J.E. Cohen, A. Phadke, H. Liu, J.A. Ellis, R. Foisner, C.L. Stewart, P.S. Zammit, and T.A. Partridge. 2013. Defective skeletal muscle growth in lamin A/C-deficient mice is rescued by loss of Lap2α. *Hum. Mol. Genet.* 22:2852–2869. <http://dx.doi.org/10.1093/hmg/ddt135>

Collas, P., E.G. Lund, and A.R. Oldenburg. 2014. Closing the (nuclear) envelope on the genome: How nuclear lamins interact with promoters and modulate gene expression. *BioEssays*. 36:75–83. <http://dx.doi.org/10.1002/bies.201300138>

Collins, C.A., I. Olsen, P.S. Zammit, L. Heslop, A. Petrie, T.A. Partridge, and J.E. Morgan. 2005. Stem cell function, self-renewal, and behavioral heterogeneity of cells from the adult muscle satellite cell niche. *Cell*. 122:289–301. <http://dx.doi.org/10.1016/j.cell.2005.05.010>

Delest, A., T. Sexton, and G. Cavalli. 2012. Polycomb: a paradigm for genome organization from one to three dimensions. *Curr. Opin. Cell Biol.* 24:405–414. <http://dx.doi.org/10.1016/j.cob.2012.01.008>

Dialynas, G., K.M. Flannery, L.N. Zirbel, P.L. Nagy, K.D. Mathews, S.A. Moore, and L.L. Wallrath. 2012. LMNA variants cause cytoplasmic distribution of nuclear pore proteins in *Drosophila* and human muscle. *Hum. Mol. Genet.* 21:1544–1556. <http://dx.doi.org/10.1093/hmg/ddr592>

Favreau, C., D. Higuier, J.C. Courvalin, and B. Buendia. 2004. Expression of a mutant lamin A that causes Emery-Dreifuss muscular dystrophy inhibits in vitro differentiation of C2C12 myoblasts. *Mol. Cell. Biol.* 24:1481–1492. <http://dx.doi.org/10.1128/MCB.24.4.1481-1492.2004>

Fredriksson, S., M. Gullberg, J. Jarvius, C. Olsson, K. Pietras, S.M. Gústafsdóttir, A. Ostman, and U. Landegren. 2002. Protein detection using proximity-dependent DNA ligation assays. *Nat. Biotechnol.* 20:473–477. <http://dx.doi.org/10.1038/nbt0502-473>

Frock, R.L., B.A. Kudlow, A.M. Evans, S.A. Jameson, S.D. Hauschka, and B.K. Kennedy. 2006. Lamin A/C and emerin are critical for skeletal muscle satellite cell differentiation. *Genes Dev.* 20:486–500. <http://dx.doi.org/10.1101/gad.1364906>

Gruenbaum, Y., and R. Foisner. 2015. Lamins: nuclear intermediate filament proteins with fundamental functions in nuclear mechanics and genome regulation. *Annu. Rev. Biochem.* 84:131–164. <http://dx.doi.org/10.1146/annurev-biochem-060614-034115>

Gruenbaum, Y., Y. Landesman, B. Drees, J.W. Bare, H. Saumweber, M.R. Paddy, J.W. Sedat, D.E. Smith, B.M. Benton, and P.A. Fisher. 1988. *Drosophila* nuclear lamin precursor Dm0 is translated from either of two developmentally regulated mRNA species apparently encoded by a single gene. *J. Cell Biol.* 106:585–596. <http://dx.doi.org/10.1083/jcb.106.3.585>

Harr, J.C., T.R. Luperchio, X. Wong, E. Cohen, S.J. Wheelan, and K.L. Reddy. 2015. Directed targeting of chromatin to the nuclear lamina is mediated by chromatin state and A-type lamins. *J. Cell Biol.* 208:33–52. <http://dx.doi.org/10.1083/jcb.201405110>

He, D.C., J.A. Nickerson, and S. Penman. 1990. Core filaments of the nuclear matrix. *J. Cell Biol.* 110:569–580. <http://dx.doi.org/10.1083/jcb.110.3.569>

Hozák, P., A.M. Sasseville, Y. Raymond, and P.R. Cook. 1995. Lamin proteins form an internal nucleoskeleton as well as a peripheral lamina in human cells. *J. Cell Sci.* 108:635–644.

Huang, W., B.T. Sherman, and R.A. Lempicki. 2009. Systematic and integrative analysis of large gene lists using DAVID bioinformatics resources. *Nat. Protoc.* 4:44–57. <http://dx.doi.org/10.1038/nprot.2008.211>

Jahn, D., S. Schramm, M. Schnölzer, C.J. Heilmann, C.G. de Koster, W. Schütz, R. Benavente, and M. Alsheimer. 2012. A truncated lamin A in the *Lmna*<sup>-/-</sup> mouse line: Implications for the understanding of laminopathies. *Nucleus*. 3:463–474. <http://dx.doi.org/10.4161/nucl.21676>

- Juan, A.H., A. Derfoul, X. Feng, J.G. Ryall, S. Dell'Orso, A. Pasut, H. Zare, J.M. Simone, M.A. Rudnicki, and V. Sartorelli. 2011. Polycomb EZH2 controls self-renewal and safeguards the transcriptional identity of skeletal muscle stem cells. *Genes Dev.* 25:789–794. <http://dx.doi.org/10.1101/gad.2027911>
- Kind, J., and B. van Steensel. 2014. Stochastic genome-nuclear lamina interactions: Modulating roles of lamin A and BAF. *Nucleus.* 5:124–130. <http://dx.doi.org/10.4161/nucl.28825>
- Kolb, T., K. Maass, M. Hergt, U. Aebi, and H. Herrmann. 2011. Lamin A and lamin C form homodimers and coexist in higher complex forms both in the nucleoplasmic fraction and in the lamina of cultured human cells. *Nucleus.* 2:425–433. <http://dx.doi.org/10.4161/nucl.2.5.17765>
- Lanzuolo, C. 2012. Epigenetic alterations in muscular disorders. *Comp. Funct. Genomics.* 2012:256892. <http://dx.doi.org/10.1155/2012/256892>
- Lanzuolo, C., and V. Orlando. 2012. Memories from the Polycomb group proteins. *Annu. Rev. Genet.* 46:561–589. <http://dx.doi.org/10.1146/annurev-genet-110711-155603>
- Lanzuolo, C., V. Roue, J. Dekker, F. Bantignies, and V. Orlando. 2007. Polycomb response elements mediate the formation of chromosome higher-order structures in the Bithorax complex. *Nat. Cell Biol.* 9:1167–1174. <http://dx.doi.org/10.1038/ncb1637>
- Lee, T.I., R.G. Jenner, L.A. Boyer, M.G. Guenther, S.S. Levine, R.M. Kumar, B. Chevalier, S.E. Johnstone, M.F. Cole, K. Isono, et al. 2006. Control of developmental regulators by Polycomb in human embryonic stem cells. *Cell.* 125:301–313. <http://dx.doi.org/10.1016/j.cell.2006.02.043>
- Lo Sardo, F., C. Lanzuolo, F. Comoglio, M. De Bardi, R. Paro, and V. Orlando. 2013. PcG-mediated higher-order chromatin structures modulate replication programs at the *Drosophila* BX-C. *PLoS Genet.* 9:e1003283. <http://dx.doi.org/10.1371/journal.pgen.1003283>
- Lund, E., A.R. Oldenburg, E. Delbarre, C.T. Freberg, I. Duband-Goulet, R. Eskeland, B. Buendia, and P. Collas. 2013. Lamin A/C-promoter interactions specify chromatin state-dependent transcription outcomes. *Genome Res.* 23:1580–1589. <http://dx.doi.org/10.1101/gr.159400.113>
- Masny, P.S., U. Bengtsson, S.A. Chung, J.H. Martin, B. van Engelen, S.M. van der Maarel, and S.T. Winokur. 2004. Localization of 4q35.2 to the nuclear periphery: Is FSHD a nuclear envelope disease? *Hum. Mol. Genet.* 13:1857–1871. <http://dx.doi.org/10.1093/hmg/ddh205>
- Mattout, A., B.L. Pike, B.D. Towbin, E.M. Bank, A. Gonzalez-Sandoval, M.B. Stadler, P. Meister, Y. Gruenbaum, and S.M. Gasser. 2011. An EDMD mutation in *C. elegans* lamin blocks muscle-specific gene relocation and compromises muscle integrity. *Curr. Biol.* 21:1603–1614. <http://dx.doi.org/10.1016/j.cub.2011.08.030>
- McCord, R.P., A. Nazario-Toole, H. Zhang, P.S. Chines, Y. Zhan, M.R. Erdos, F.S. Collins, J. Dekker, and K. Cao. 2013. Correlated alterations in genome organization, histone methylation, and DNA-lamin A/C interactions in Hutchinson-Gilford progeria syndrome. *Genome Res.* 23:260–269. <http://dx.doi.org/10.1101/gr.138032.112>
- Méjat, A., V. Decostre, J. Li, L. Renou, A. Kesari, D. Hantaï, C.L. Stewart, X. Xiao, E. Hoffman, G. Bonne, and T. Misteli. 2009. Lamin A/C-mediated neuromuscular junction defects in Emery-Dreifuss muscular dystrophy. *J. Cell Biol.* 184:31–44. <http://dx.doi.org/10.1083/jcb.200811035>
- Melcon, G., S. Kozlov, D.A. Cutler, T. Sullivan, L. Hernandez, P. Zhao, S. Mitchell, G. Nader, M. Bakay, J.N. Rottman, et al. 2006. Loss of emerin at the nuclear envelope disrupts the Rb1/E2F and MyoD pathways during muscle regeneration. *Hum. Mol. Genet.* 15:637–651. <http://dx.doi.org/10.1093/hmg/ddi479>
- Moir, R.D., M. Yoon, S. Khuon, and R.D. Goldman. 2000. Nuclear lamins A and B1: Different pathways of assembly during nuclear envelope formation in living cells. *J. Cell Biol.* 151:1155–1168. <http://dx.doi.org/10.1083/jcb.151.6.1155>
- Muñoz-Alarcón, A., M. Pavlovic, J. Wismar, B. Schmitt, M. Eriksson, P. Kylsten, and M.S. Dushay. 2007. Characterization of lamin mutation phenotypes in *Drosophila* and comparison to human laminopathies. *PLoS One.* 2:e532. <http://dx.doi.org/10.1371/journal.pone.0000532>
- Oldenburg, A.R., E. Delbarre, B. Thiede, C. Vigouroux, and P. Collas. 2014. Deregulation of Fragile X-related protein 1 by the lipodystrophic lamin A p.R482W mutation elicits a myogenic gene expression program in preadipocytes. *Hum. Mol. Genet.* 23:1151–1162. <http://dx.doi.org/10.1093/hmg/ddt509>
- Otsu, N. 1979. A threshold selection method from gray-level histograms. *New Afr.* 9:62–66. *IEEE Trans. Syst. Man Cybern.* 8:62–66. <http://dx.doi.org/10.1109/TSMC.1979.4310076>
- Palacios, D., C. Mozzetta, S. Consalvi, G. Caretti, V. Saccone, V. Proserpio, V.E. Marquez, S. Valente, A. Mai, S.V. Forcales, et al. 2010. TNF/p38/polycomb signaling to Pax7 locus in satellite cells links inflammation to the epigenetic control of muscle regeneration. *Cell Stem Cell.* 7:455–469. <http://dx.doi.org/10.1016/j.stem.2010.08.013>
- Paro, R., and B. Zink. 1993. The Polycomb gene is differentially regulated during oogenesis and embryogenesis of *Drosophila melanogaster*. *Mech. Dev.* 40:37–46. [http://dx.doi.org/10.1016/0925-4773\(93\)90086-D](http://dx.doi.org/10.1016/0925-4773(93)90086-D)
- Relaix, F., D. Rocancourt, A. Mansouri, and M. Buckingham. 2004. Divergent functions of murine Pax3 and Pax7 in limb muscle development. *Genes Dev.* 18:1088–1105. <http://dx.doi.org/10.1101/gad.301004>
- Riemer, D., and K. Weber. 1994. The organization of the gene for *Drosophila* lamin C: limited homology with vertebrate lamin genes and lack of homology versus the *Drosophila* lamin Dmo gene. *Eur. J. Cell Biol.* 63:299–306.
- Röder, R.A., K. Weber, and M. Osborn. 1989. Differential timing of nuclear lamin A/C expression in the various organs of the mouse embryo and the young animal: A developmental study. *Development.* 105:365–378.
- Rosenblatt, J.D., A.I. Lunt, D.J. Parry, and T.A. Partridge. 1995. Culturing satellite cells from living single muscle fiber explants. *In Vitro Cell. Dev. Biol. Anim.* 31:773–779. <http://dx.doi.org/10.1007/BF02634119>
- Russ, J.C. 2011. The Image Processing Handbook. Sixth edition. Taylor & Francis, New York. 885 pp.
- Satijn, D.P., M.J. Gunster, J. van der Vlag, K.M. Hamer, W. Schul, M.J. Alkema, A.J. Saurin, P.S. Freemont, R. van Driel, and A.P. Otte. 1997. RING1 is associated with the Polycomb group protein complex and acts as a transcriptional repressor. *Mol. Cell Biol.* 17:4105–4113. <http://dx.doi.org/10.1128/MCB.17.7.4105>
- Scaffidi, P., and T. Misteli. 2008. Lamin A-dependent misregulation of adult stem cells associated with accelerated ageing. *Nat. Cell Biol.* 10:452–459. <http://dx.doi.org/10.1038/ncb1708>
- Schiaffino, S., K.A. Dyar, S. Ciciliot, B. Blaauw, and M. Sandri. 2013. Mechanisms regulating skeletal muscle growth and atrophy. *FEBS J.* 280:4294–4314. <http://dx.doi.org/10.1111/febs.12253>
- Schuettengruber, B., A.M. Martinez, N. Iovino, and G. Cavalli. 2011. Trithorax group proteins: Switching genes on and keeping them active. *Nat. Rev. Mol. Cell Biol.* 12:799–814. <http://dx.doi.org/10.1038/nrm3230>
- Schulze, S.R., B. Curio-Penny, S. Speese, G. Dyalnas, D.E. Cryderman, C.W. McDonough, D. Nalbant, M. Petersen, V. Budnik, P.K. Geyer, and L.L. Wallrath. 2009. A comparative study of *Drosophila* and human A-type lamins. *PLoS One.* 4:e7564. <http://dx.doi.org/10.1371/journal.pone.0007564>
- Sezgin, M., and B. Sankur. 2004. Survey over image thresholding techniques and quantitative performance evaluation. *J. Electron. Imaging.* 13:146–168. <http://dx.doi.org/10.1117/1.1631315>
- Shimi, T., K. Pflieger, S. Kojima, C.G. Pack, I. Solovei, A.E. Goldman, S.A. Adam, D.K. Shumaker, M. Kinjo, T. Cremer, and R.D. Goldman. 2008. The A- and B-type nuclear lamin networks: Microdomains involved in chromatin organization and transcription. *Genes Dev.* 22:3409–3421. <http://dx.doi.org/10.1101/gad.1735208>
- Shumaker, D.K., T. Dechat, A. Kohlmaier, S.A. Adam, M.R. Bozovsky, M.R. Erdos, M. Eriksson, A.E. Goldman, S. Khuon, F.S. Collins, et al. 2006. Mutant nuclear lamin A leads to progressive alterations of epigenetic control in premature aging. *Proc. Natl. Acad. Sci. USA.* 103:8703–8708. <http://dx.doi.org/10.1073/pnas.0602569103>
- Šmigová, J., P. Juda, D. Cmarko, and I. Raška. 2011. Fine structure of the “PcG body” in human U-2 OS cells established by correlative light-electron microscopy. *Nucleus.* 2:219–228. <http://dx.doi.org/10.4161/nucl.2.3.15737>
- Solovei, I., A.S. Wang, K. Thanisch, C.S. Schmidt, S. Krebs, M. Zwerger, T.V. Cohen, D. Devys, R. Foisner, L. Peichl, et al. 2013. LBR and lamin A/C sequentially tether peripheral heterochromatin and inversely regulate differentiation. *Cell.* 152:584–598. <http://dx.doi.org/10.1016/j.cell.2013.01.009>
- Stewart, C., and B. Burke. 1987. Teratocarcinoma stem cells and early mouse embryos contain only a single major lamin polypeptide closely resembling lamin B. *Cell.* 51:383–392. [http://dx.doi.org/10.1016/0092-8674\(87\)90634-9](http://dx.doi.org/10.1016/0092-8674(87)90634-9)
- Sullivan, T., D. Escalante-Alcalde, H. Bhatt, M. Anver, N. Bhat, K. Nagashima, C.L. Stewart, and B. Burke. 1999. Loss of A-type lamin expression compromises nuclear envelope integrity leading to muscular dystrophy. *J. Cell Biol.* 147:913–920. <http://dx.doi.org/10.1083/jcb.147.5.913>
- Tolhuis, B., M. Blom, R.M. Kerkhoven, L. Pagie, H. Teunissen, M. Nieuwland, M. Simonis, W. de Laat, M. van Lohuizen, and B. van Steensel. 2011. Interactions among Polycomb domains are guided by chromosome architecture. *PLoS Genet.* 7:e1001343. <http://dx.doi.org/10.1371/journal.pgen.1001343>
- Trapnell, C., A. Roberts, L. Goff, G. Pertea, D. Kim, D.R. Kelley, H. Pimentel, S.L. Salzberg, J.L. Rinn, and L. Pachter. 2012. Differential gene and transcript expression analysis of RNA-seq experiments with TopHat and Cufflinks. *Nat. Protoc.* 7:562–578. <http://dx.doi.org/10.1038/nprot.2012.016>
- Wang, J., R.M. Kumar, V.J. Biggs, H. Lee, Y. Chen, M.H. Kagey, R.A. Young, and C. Abate-Shen. 2011. The Mx1 homeoprotein recruits Polycomb to

- the nuclear periphery during development. *Dev. Cell.* 21:575–588. <http://dx.doi.org/10.1016/j.devcel.2011.07.003>
- Wang, X.-F., D.-S. Huang, and H. Xu. 2010. An efficient local Chan-Vese model for image segmentation. *Pattern Recognit.* 43:603–618. <http://dx.doi.org/10.1016/j.patcog.2009.08.002>
- Woodhouse, S., D. Pugazhendhi, P. Brien, and J.M. Pell. 2013. Ezh2 maintains a key phase of muscle satellite cell expansion but does not regulate terminal differentiation. *J. Cell Sci.* 126:565–579. <http://dx.doi.org/10.1242/jcs.114843>
- Zaremba-Czogalla, M., M. Dubińska-Magiera, and R. Rzepecki. 2011. Laminopathies: The molecular background of the disease and the prospects for its treatment. *Cell. Mol. Biol. Lett.* 16:114–148. <http://dx.doi.org/10.2478/s11658-010-0038-9>
- Zwerger, M., D.E. Jaalouk, M.L. Lombardi, P. Isermann, M. Mauermann, G. Dialynas, H. Herrmann, L.L. Wallrath, and J. Lammerding. 2013. Myopathic lamin mutations impair nuclear stability in cells and tissue and disrupt nucleo-cytoskeletal coupling. *Hum. Mol. Genet.* 22:2335–2349. <http://dx.doi.org/10.1093/hmg/ddt079>